From the Department of Clinical Science,
Intervention and Technology
Karolinska Institutet, Stockholm, Sweden

RADIATION DOSE-, CONTRAST MEDIA- AND IMAGE QUALITY OPTIMIZATION IN COMPUTED TOMOGRAPHY

Daniel Thor

Karolinska Institutet

Stockholm 2019

Published by Karolinska Institutet.
Printed by Eprint AB 2019

ISBN 978-91-7831-572-7

Radiation Dose-, Contrast Media- and Image Quality Optimization in Computed Tomography
THESIS FOR DOCTORAL DEGREE (Ph.D.)

By

Daniel Thor

Principal Supervisor:
Associate Professor Torkel Brismar
Karolinska Institutet
Department of Clinical Science, Intervention and Technology

Co-supervisor(s):
Associate Researcher Gavin Poludniowski
Karolinska Institutet
Department of Oncology-Pathology

Associate Professor Marcus Söderberg
Lund University
Department of Translational Medicine
Medical Radiation Physics

Opponent:
Professor Magnus Båth
University of Gothenburg
Department of Department of Radiation Physics

Examination Board:
Associate Professor Tomas Bjerner
Uppsala University
Department of Surgical Sciences

Professor Anders Sundin
Uppsala University
Department of Surgical Sciences

Associate Professor Ragnar Kullenberg
University of Gothenburg
Halland Hospital, Halmstad

ABSTRACT

Computed tomography (CT) was introduced to medicine in the early 1970s, which brought slice imaging into wide use for the first time. Today, CT is an essential part of radiological diagnostics, and is used for a wide range of clinical applications. One downside of CT imaging is the health risks related to the ionizing radiation. In the 80s it was believed that CT would soon be replaced completely by MRI due, in part, to the ionizing radiation required in CT. A further downside are the health risks related to the use of iodine-based contrast media. Both radiation- and contrast media dose have a trade-off with image quality. However, many technical advances have been made, and progress is still ongoing, to improve and broaden the applications of CT. Such advances necessitate a re-evaluation of imaging protocols and continued optimization of radiation dose, contrast media dose and imaging quality. This is the subject of this PhD project.

Study I: The aim of this study was to evaluate the potential of low-kV dual-source (DS) and dual-energy (DE) to reduce CM-doses while maintaining soft-tissue and iodine CNR in phantoms of varying size, and to quantify the corresponding radiation dose increases. It was found that low-kV dual-source imaging could be used to reduce CM doses by 44–53% with maintained iodine-, soft tissue- and other materials CNR in a wide range of abdominal sizes, to the cost of about 20–100% increased radiation dose, depending on size. The dual-energy technique allowed a reduction of CM dose by 20% at similar radiation dose as the standard 120 kV protocol.

Study II: The aim of this study was to implement and evaluate a scanning regimen, based on the results from Study I, to reduce CM-doses for patients believed to be at risk of CIN. It was concluded that the protocols from Study I could be used to reduce CM doses by 40–50%, depending on patient size, with maintained CNR in patients with a BMI-range of 15–36 kg/m^2. The size-specific dose estimates increased by 70%.

Study III: The aim of this study was to compare the outcome in image noise and radiation dose in the subsequent CT scan following a single anterior-posterior (AP) vs a combined lateral plus AP (LAT+AP) localizer when using automatic tube-current modulation (ATCM). The results suggested that using LAT+AP localizer yields more consistent noise and radiation dose than a single AP. The effect was small, except for a subgroup of females with laterally protruding breast tissue, which may have been overexposed by about 57% in the thorax region.

Study IV: The aim of this study was to evaluate if standard-dose CT can be replaced with low-dose CT for characterization of non-specific findings bone in scintigraphy. Based on these results, sub-mSv CT seems feasible for morphological characterization of skeletal changes in areas with increased tracer uptake on bone scintigraphy, although a larger study is needed.

LIST OF SCIENTIFIC PAPERS

The four papers included in this thesis are listed below. They will be referred to by their roman numerals.

I. *Low tube voltage dual source computed tomography to reduce contrast media doses in adult abdomen examinations: A phantom study*
Thor D., Brismar T.B., and Fischer M.A., Medical Physics, 2015. 42(9): p. 5100-9.

II. *Dual source abdominal computed tomography: the effect of reduced X-ray tube voltage and intravenous contrast media dosage in patients with reduced renal function*.
Svensson, A.*, Thor D.*, Fisher M.A., Brismar T.B., Acta Radiologica, 2019. 60(3): p. 293-300. *shared first authorship

III. *Effect of localizer orientation on ATCM consistency*
Thor D., Poludniowski G., Söderberg M., Brismar T.B., Manuscript

IV. *Is sub-mSv CT for evaluation of non-specific findings in bone scintigraphy of oncological patients feasible?*
Zakko Y., Thor D., Savitcheva I., Sundvall A., Wassberg C., Koskinen S.K., and Axelsson R., Acta Radiologica, 2019. E-pub ahead of print.

CONTENTS

LIST OF ABBREVIATIONS

AP	Anterior-posterior
ATCM	Automatic tube-current modulation
AUC	Area under the receiver operator characteristics curve
BMI	Body mass index
CM	Contrast media
CI	Confidence interval
CIN	Contrast-induced nephropathy
CNR	Contrast-to-noise ratio
CNRD	Dose-weighted contrast-to-noise ratio
CT	Computed tomography
CTDI	Computed tomography dose index
DE	Dual energy
DICOM	Digital imaging and communications in medicine
DLP	Dose-length product
DS	Dual source
D_w	Water equivalent diameter
ED	Effective dose
eGFR	Estimated glomerular filtration rate
HU	Hounsfield value
LAT	Lateral
LCD	Low contrast detectability
MRI	Magnetic resonance imaging
MTF	Modulation transfer function
mAs	Milliampere-second
mAs_{eff}	Effective milliampere-second
NPS	Noise power spectrum
nRMSE	Normalized root mean squared error
PC-AKI	Post-contrast acute kidney injury
ROC	Receiver operator characteristics
SS	Single source

SSDE	Size-specific dose estimate
ROI	Region of interest
Z	Atomic number
Z_{eff}	Effective atomic number

1 INTRODUCTION

The first clinical computed tomography (CT) system was installed at London's Atkinson-Morley Hospital in 1971, however research dates back as early as 1940 [1]. Since the introduction of CT, tremendous advancements in the technology have been seen: most notably in scan times (minimum effective scan time has decreased from about 300 to 0.15 s), resolution (slice thickness has decreased from about 13 to 0.6 mm and in-plane spatial resolution increased from 3 to 25 linepairs/cm) and power (from about 2 kW to 100 kW) [2].

One of the most important benefits of CT is that the tomographic method offers much higher contrast than the conventional radiograph, in which distinct anatomical structures are superimposed into one projection. The main competitor to CT is magnetic resonance imaging (MRI) which has superior soft tissue contrast (important in imaging of brain, tendons/ligaments, nerves etc.), and does not use ionizing radiation. CT, on the other hand, has higher resolution (important in imaging of lung, bone, etc.) and much faster scan times (which translates into lower cost and greater availability). CT, however, can also be a good choice for soft tissue imaging when used in combination with contrast media (CM).

In the 80s it was believed that CT would soon be replaced completely by MRI due, in part, to the ionizing radiation required in CT [3]. A further downside are the health risks related to the use of iodine-based CM. However, many technical advances have been made, and progress is still ongoing, to improve and broaden the applications of CT. Some notable advances have been: automatic tube-current modulation (ATCM), detector design, x-ray spectrum optimization, dual-energy (DE)- and dual-source (DS) CT. Such advances necessitate a re-evaluation of imaging protocols and continued optimization of radiation dose, contrast media dose and imaging quality. This is the subject of this PhD project.

1.1 BASIC PRINCIPLES OF CT

CT is a tomographic modality that reconstructs a 3D map of x-ray linear attenuation coefficients in the scanned object, by measuring the transmission of x-ray at several angular orientations (typically between 500–4000 projections per rotation), at positions along the object (either by step-and-shoot, i.e. axial scanning, or by continuously moving the table, i.e. spiral scanning). Since the incident radiation intensity is known, the linear attenuation for each ray path can be calculated using the Beer-Lamberts law, which for monochromatic radiation ignoring scatter, is equal to

$$I = I_0 e^{-\mu d} \tag{1}$$

where μ is the attenuation coefficient of a material of thickness d, I_0 and I is the number of photons entering and exiting the object respectively. The attenuation coefficient depends strongly on material density and atomic number and on photon energy (see section 1.2.1). In a medical context however, the radiation is produced in an x-ray tube and is therefore made up of a spectrum of energies (Figure 1), and currently used scintillator detectors[1] are measuring the radiation intensity, not the number of photons or the energy of the photons.[2] This means that the energy dependence is not captured by the measurements and need to be corrected for in order to not introduce artifacts in the image.

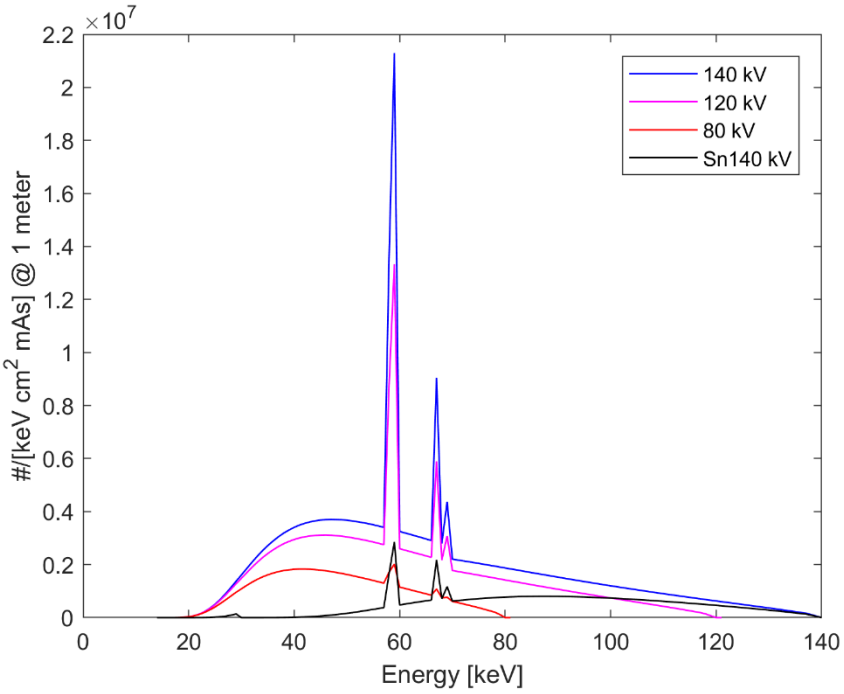

FIGURE 1: Examples of CT spectrums at three different tube voltages (kV), and with additional heavy filtering (Sn140 kV). The spectrums are filtered with 6 mm Al or 6 mm Al plus 0.4 mm Sn in the Sn140 kV example (corresponding to the added filter used in dual-source dual-energy mode, where a small spectral overlap between the 80 and 140 kV spectrums is desired). The effect of filtering with a high atomic number, such as Sn, is to right-shift the spectrum due to the photoelectric effect (see section 1.2.1). The spectrum data is calculated using the software SpekCalc [4].

The CT image is generated in the following manner. Via the relationship in equation 1, an attenuation profile for each projection is acquired which can be reconstructed into an image of the object, using one of the main reconstruction techniques: filtered back projection or

[1] Ignoring photon-counting detectors which have seen great progress, and is close to reaching clinical implementation.

[2] These factors mean that the measurement situation of expression (1) turns into

$$I = \int_0^{E_{max}} I_0(E) e^{-\int_0^d \mu(E,s)ds}\, dE$$

where $\mu(E,s)$ indicate that μ depends on energy and position along d, $I_0(E)$ is the intensity for each energy and I is the intensity exiting an object of thickness d.

iterative reconstruction. Each voxel in the image is assigned a value corresponding to the measured mean attenuation in that voxel, scaled to the attenuation of water. These values are called CT-numbers, and have the unit Hounsfield unit (HU) which is defined as

$$HU = \frac{\mu(x, y, z) - \mu_{water}}{\mu_{water}} \times 1000 \quad (2)$$

where $\mu(x,y,z)$ is the mean attenuation in the voxel at position (x,y,z) and μ_{water} is the attenuation of water. In the HU-scale, water will per definition have the value 0 HU and air will have −1000 HU (since the attenuation of air is approximately zero).[3] There are several benefits of this scale. Firstly, displaying the actual μ-value would be clinically meaningless, both since it has no intuitive interpretation and because it is energy dependent and would therefore change based on spectrum. Secondly, that it emphasizes small deviations from water i.e. small differences in soft tissue attenuation (since tissue is mainly water). Thirdly, water is an easily available material for calibration. A further thing to note about the HU-scale is that the range is very large; the difference between air and bone or metal can be several thousand HU. It is therefore not possible to display all these values as grayscale values on a typical monitor, nor would it be possible for the human vision system to distinguish the resulting small differences in grayscale of tissues. For this reason, CT images are viewed using a technique called windowing. Windowing mean that the entire grayscale is assigned to a specific "window", i.e. a range of CT-numbers of interest that is manually adjusted by the viewer.

1.2 CONTRAST MEDIA

Contrast media (CM) – as indicated by the name – increase image contrast and adds functional information since uptake of CM differs between tissues, often changes where there is pathology and varies dynamically with elapsed time from administration.

1.2.1 Physical Principle of CM

The principle behind CM used for CT is that they contain atoms with high atomic numbers (Z) which increase the attenuation of x-rays and therefore the image contrast between tissues with different amounts of uptake (e.g. vessels/surrounding tissue, organ/tumor etc.). The most commonly used CM contain iodine (with Z=53) and is typically injected intra-venously into the patient [5].

In the x-ray energy range (about 30–150 keV), the two main modes of attenuation are Compton and photoelectric effect. The Compton linear attenuation coefficient is proportional to $\frac{N_A Z}{A}\sigma_e\,\rho$ (in which N_A is Avogadro's constant, A is the number of grams per mole, σ_e is

[3] Note that since water density changes with temperature (the water temperature used in calibration is room temperature), and due to the imperfect correction for x-ray spectrum changes (beam-hardening), the in-vivo value of water will differ slightly from zero.

the total Klein-Nishina cross-section per electron and ρ is the density), whereas photoelectric effect is proportional to $(\frac{Z}{h\nu})^3\rho$ (where hν is the photon energy) [6]. Since $\frac{N_A Z}{A}\rho$ is equal to the electron density of the material, Compton can roughly be said to be proportional to the density of the object, approximately Z-independent, and with a weak decrease with increasing x-ray energies (due to the σ_e-factor). Photoelectric effect on the other hand increases strongly with increasing atomic number and decreasing photon energies. Compton is the predominant interaction throughout the x-ray energy spectrum for all materials with a Z of below about 10–15, whereas photoelectric effect dominates at all x-ray energies for Z of about >15–25 [6]. The effective atomic number (Z_{eff}) of human soft tissue (excluding fat) is close to water and varies very little: water, blood, brain-, heart-, kidney-, liver-, lung-, muscle-, pancreas- and spleen-tissue are all within the Z_{eff}-interval of about 7.33-7.55 [7, 8], which means that image contrast between these objects, or between these objects and lesions of similar Z_{eff}, will almost entirely be determined by their often very small density differences, unless CM is used. Some relevant bodily materials with deviating Z_{eff} are fat and non-soft-tissue objects like bone and calcium-based kidney stones with Z_{eff} of about 6, 9–13 and 11–15 respectively [7, 9]). Figure 2 shows the mass attenuation coefficients for iodine, bone and water (left side) and the estimated more realistic example of attenuation coefficients when taking tissue density and CM concentrations into account (right side).

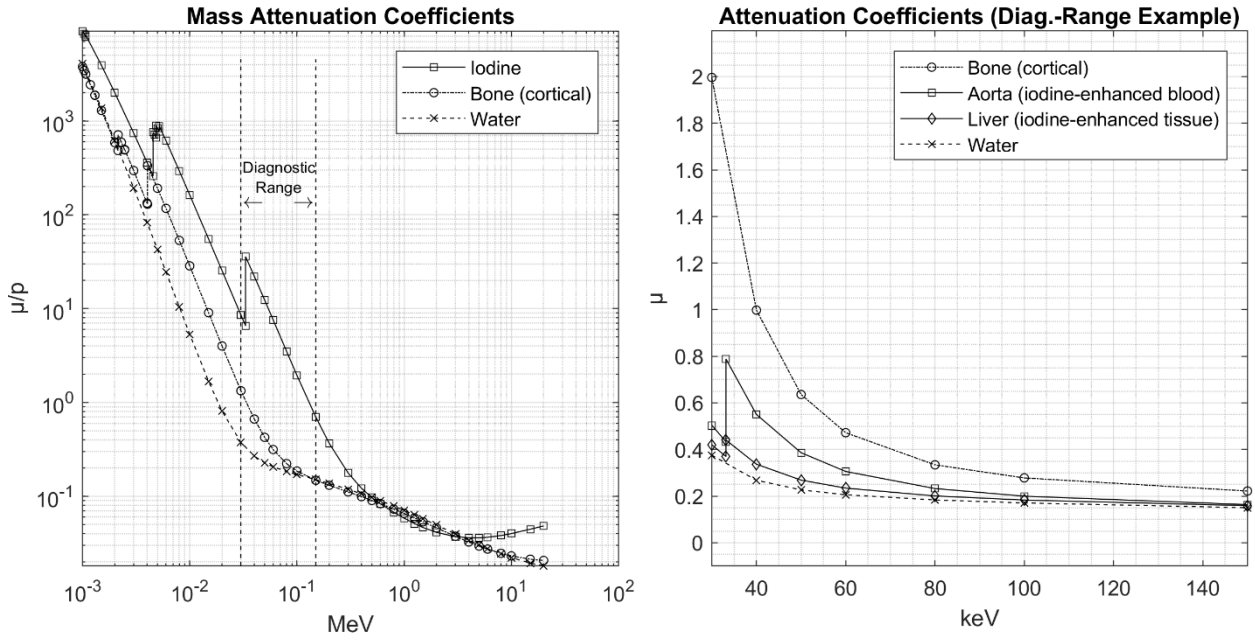

FIGURE 2: Left: mass attenuation coefficients for iodine, bone (cortical) and water (plotted using data from NIST [10]). Right: example of estimated attenuation coefficient in the diagnostic energy range using typical values of tissue density and CM concentrations (in venous phase). The attenuation coefficient for aorta and liver is calculated as the sum of the iodine- plus baseline attenuation of blood and tissue respectively. The unenhanced blood and tissue lines (not shown in the graph) lay slightly above water. By using the definition of CT-numbers for the energy of about 70–80 keV (approximate mean energy of a 120 kV spectra), one would from this graph get CT-numbers of roughly 1000, 300, 100 and 0 HU for bone, aorta, liver and water respectively.

1.2.2 Adverse Effects of Iodine-Based CM

One of the drawbacks of iodine-based CM is that they can have adverse effects, such as: allergic reactions, affect thyroid function and cause kidney damage [11, 12]. The current American College of Radiology guidelines define PC-AKI (post-contrast acute kidney injury) as "a general term used to describe a sudden deterioration in renal function that occurs within 48 hours following the intra-vascular administration of iodinated contrast medium", and CIN (contrast-induced nephropathy), also known as CI-AKI (contrast-induced acute kidney injury), as "a specific term used to describe a sudden deterioration in renal function that is caused by the intravascular administration of iodinated contrast medium" [13]. This means that CIN is a subgroup of PC-AKI, and that the main difference is that CIN implies a causal relationship whereas PC-AKI only implies correlation. The incidence of PC-AKI has been estimated to be about 5% [14, 15]. In those studies, patients with reduced kidney function and patients with diabetes were at increased risk (odds ratio 2.26 and 3.1 respectively) [14]. There is some controversy about whether there is a causal relationship (CIN) or merely a correlation (PC-AKI) between CM and kidney injury. Some publications have used a control group of patients with matched risk factors (propensity score matching) who were examined without CM and found no difference in frequency of incidences [16, 17]. However, according to the Swedish guidelines [12] (by Svensk uroradiologisk förenings kontrastmedelsgrupp), there are several methodological problems with these studies – the main one being a large selection bias: 90% of the non-CM patients were in-patients and therefore at higher baseline risk – meanwhile other studies with control groups have found an increased risk for the CM group. The guidelines conclude that CIN do exist but that the risk probably is smaller than previously believed, given that preventive measures are used. The Swedish guidelines state that the CM dose always ought to be as low as possible without risking the diagnostic quality (which is in agreement with international recommendations); and that dosage should be based on weight and take estimated glomerular filtration rate (eGFR) into account. If the patient is believed to be at risk of CIN the CM dose should be reduced so that the ratio of the CM dose to the eGFR is smaller than 0.5 (gI/eGFR<0.5), which is typically half that of a patient without risk factors.

1.3 RADIATION

1.3.1 Radiation Dose in CT

The general definition of absorbed dose (also called energy dose) is: absorbed energy divided by tissue mass, which has the unit Gray (Gy, [J/kg]). Several metrics and measurement methodologies have been used through the years to measure radiation doses in CT. Today the Computed Tomography Dose Index (CTDI) is a standardized metric used for quality assurance, optimization, diagnostic reference levels, and as a dosimetric starting-point to estimate patient doses. The measurement is performed via $CTDI_{100}$, which is defined by the International Electrotechnical Commission (IEC) as

$$CTDI_{100} = \int_{-50\,mm}^{+50\,mm} \frac{D(z)}{N \times T} dz \quad (3)$$

for nominal detector widths ≤ 40 mm[4], where *D(z)* is the dose profile along the z-plane measured in a standardized phantom, *(N×T)* is the nominal detector width (*N* = number of detector rows, *T* = width of one detector row) [18][5]. The phantoms are plexiglass cylinders of 32- and 16 cm diameter which are intended to correspond to the absorption properties of an adult abdomen and head. Due to the dose difference of the central and peripheral part of the phantom, the weighted $CTDI_{100}$ ($CTDI_w$) is calculated as

$$CTDI_w = \frac{1}{3} CTDI_{100,c} + \frac{2}{3} CTDI_{100,p} \quad (4)$$

where the indices *c* and *p* refer to a measurement in the central and peripheral part of the phantom respectively. CT scanners have a look-up table of $CTDI_w$:s for all combinations of acquisition parameters, and actual measurements are only done in calibration and quality assurance. The displayed and reported dose index, however, are always in terms of the volume $CTDI_w$ ($CTDI_{vol}$) which is defined as

$$CTDI_{vol} = \frac{CTDI_w}{pitch} \quad (5)$$

i.e. corrected for pitch, where pitch is defined as the table feed per rotation divided by *(N×T)*.

Effective dose (ED) is a concept introduced by the International Commission on Radiological Protection (ICRP) as a radiation protection quantity. It can be used to compare the radiation detriment from non-homogenous or partial-body exposures to that of a homogenous whole-body exposure to ionizing radiation (i.e. the aim is that the numerical value of ED for an arbitrary exposure should, statistically, yield the same expected detriment as a homogenous whole-body dose of the same numerical value). Detriment in this context refer to stochastic effects: cancer (almost exclusively) and heritable effects (to a very small extent). It is calculated as

$$ED = \sum_T w_T \sum_R w_R D_{T,R} \quad (6)$$

(where *T* is a tissue or organ, w_T, the tissue weighting-factor and $w_R D_{T,R}$ is the equivalent dose from radiation *R*), in the unit sievert (Sv [J/kg]) [19]. The tissue weighting factors are defined by ICRP committees based on biological and epidemiological evidence of the health-

---

[4] For widths > 40 mm it is defined as $CTDI_{100} = \int_{-50\,mm}^{+50\,mm} \frac{D_{Ref}(z)}{(N\times T)_{Ref}} dz \times \frac{CTDI_{free\ in\ air,N\times T}}{CTDI_{free\ in\ air,Ref}}$
where the subscript *Ref* refers to a reference measurement with *(N×T)* equal to 20 mm (or the largest available setting < 20 mm), and $CTDI_{free\ in\ air}$ refers to a measurement in iso-center without phantom.

[5] Note that $CTDI_{100}$ is not actually a dose measurement, rather it is an integration of the dose profile for one stationary rotation normalized to *(N×T)*. Due to this normalization, $CTDI_{100}$ predicts the dose at the center of a scan-length covered by multiple rotations with a pitch of unity (pitch is defined as the table feed per rotation divided by *(N×T)*).

risks of radiation, combined with considerations related to the consequences (mortality of the detriment conditions, quality of life and loss of life years). This mean that if, for example, the health outcome of radiation-induced cancers relating to a specific organ became better, the tissue weighting factor would be decreased. Further, the tissue weighting factor are age- and sex averaged. Therefore, ED should not be used for epidemiological risk assessments or specific individual risk estimations. The intended use of ED is prospective dose assessment for planning and optimization in radiological protection and to demonstrate legal compliance with dose-limits. In practice, ED from CT examinations are typically calculated using tables of conversion factors from dose-length product (DLP; defined as $CTDI_{vol}$ × scanned length) to ED for different body parts [20]. The conversion factors have been derived using Monte Carlo simulations in different mathematical phantoms, scoring the absorbed dose to the different organs and using equation 6 above. For more precise calculations, and/or for non-standard scan lengths, and/or for specific organ dose calculations, Monte Carlo based software (such as CT-Expo and CTDosimetry [21, 22]) are often used. These programs include information about relevant x-ray output parameters from most commonly used scanners models, which is used to simulate doses in a mathematical phantom or, more recently, use patient images instead of a mathematical phantom, although this latter approach requires manual intervention as no current software is able to segment all the relevant organs.

1.3.1.1 Size-Specific Dose Estimate

Because CTDI is measured in phantoms of sizes close to an adult abdomen (32 cm) and head (16 cm) made of a material of similar x-ray absorption properties as tissue, CTDI makes for a good dosimetric starting point. However, individual body sizes (and body parts) for the entire population can vary greatly from 32- and 16 cm, which has a large impact on actual organ doses. In recent years, a new CT dose metric called size-specific dose estimate (SSDE) has been proposed, and a considerable amount of work has gone into correlating doses in 32- and 16 cm phantoms with doses in arbitrary sizes [23-27]. SSDE is defined as

$$SSDE = f_{size}^{32x,16x} \times CTDI_{vol}^{32,16} \tag{7}$$

where $f_{size}^{32x,16x}$ is an empirically derived conversion factor (combining measurements and simulations) from dose in a 32- or 16 cm cylinder phantom to dose in tissue of varying elliptical sizes [24]. The two most common ways of estimating the elliptical size are via effective diameter (D_{eff}) and water-equivalent diameter (D_w). The effective diameter is the diameter of a circle whose area is equal to the area of the elliptical object, and is therefore calculated as

$$D_{eff} = \sqrt{AP \times LAT} \tag{8}$$

where AP and LAT are the anterior-posterior and lateral diameters. The water-equivalent diameter can be understood as the diameter of a water cylinder that would absorb the same average dose as the elliptical cross section, and is calculated as

$$D_w = 2\sqrt{A_w/\pi} \tag{9}$$

where A_w is the water-equivalent area, calculated as

$$A_w = \sum_i \left(\frac{\mu(x,y)_i}{\mu_{water}}\right)^{\alpha} \times A_{pixel}$$

$$= \sum_i \left(\frac{CT(x,y)_i}{1000} + 1\right)^{\alpha} \times A_{pixel} \quad (10)$$

where $\mu(x,y)$ is the attenuation coefficient of a voxel at location (x,y) in an axial slice, $CT(x,y)$ is the corresponding CT-number, A_{pixel} is the area of the pixel and a linear dependence, α=1, has been shown to be a valid assumption [25].

1.3.2 Radiation Risk

An important downside of CT is that low-dose radiation exposure (often defined as <100 mSv [28]) is believed to cause cancer. There is strong epidemiological evidence, that exposure to moderate or high radiation doses (>100 mSv) increases the incidence of solid tumors and leukemia [29, 30], however CT doses are almost always lower than this. Organ doses in CT examinations are seldom above 100 mGy[6]. $CTDI_{vol}$ for routine head scans is generally between 30–70 mGy, and for routine abdominal scans between 5–25 mGy [31, 32], meaning that brain doses of about 50 mGy and abdominal organ doses of about 15 mGy are common (in multiphase abdominal examinations doses typically become a factor 2–4 times higher).

The evidence of risks associated with low-dose radiation is difficult to assess epidemiologically due to the poor statistics of rare cases and/or to confounding variables in non-experimental study designs. As a result, the conclusions in the literature are more mixed. Therefore, extensive reviews of both mechanistic and epidemiological data are likely needed to reach any sound conclusions. The United Nations Scientific Committee on the Effects of Atomic Radiation (UNSCEAR) and The Committee on the Biological Effects of Ionizing Radiation (BEIR) of the National Research Council in USA periodically reviews the evidence. In their most recent health reports the BEIR committee "[...] judges that the balance of evidence from epidemiologic, animal, and mechanistic studies tends to favor a simple proportionate relationship at low doses between radiation dose and cancer risk. Uncertainties in this judgment are recognized and noted." [33], and the UNSCEAR committee concludes that "the current balance of available [mechanistic] evidence tends to favor a non-threshold response for the mutational component of radiation-associated cancer induction at low doses and low dose rates" [30]. The BEIR VII lifetime risk model predicts that approximately 1 person per 100 is expected to develop cancer due to a whole-body dose of 100 mSv and that, proportionally, 1 person per 1000 would develop cancer from 10 mSv.

Given the plausibility of a non-threshold response, no radiation dose can be considered risk-

[6] The conversion factor from mGy (energy dose) to mSv (equivalent dose) is 1 for photons. For the sake of this text, the magnitude of the numbers in this section can be roughly compared.

free. Therefore, the three key principles of radiological protection recommended by the ICRP is: justification, optimization and the application of dose limits (although the latter do not apply to medical exposures). The Swedish Radiation Safety Authority's regulations on medical exposures states that the extent of the examination and the radiation dose should be individually adjusted so that the needed diagnostic information is acquired with use of as low radiation dose as reasonably achievable (known as the ALARA-principle) [32].

1.4 IMAGE QUALITY

1.4.1 Low-Contrast Detectability

The ability to distinguish low-contrast objects is one of the most vital properties of CT, especially compared to conventional x-ray, and is what helped CT achieve its breakthrough [2]. This property is referred to as low-contrast detectability (LCD), and is a concept used both in quality control and optimization. There are several ways in which LCD can be assessed. In quality assurance a common metric is the so-called contrast-detail curve which quantifies the smallest visible object as a function of object contrast. In optimization and detection studies, the area (AUC) under the receiver operator characteristics (ROC) curve is a very useful metric that evaluates the ability to separate the signal from the noise.

The LCD depends mainly on the contrast between the object and background, the size of the object and the level of noise. A substantial amount of research has gone into the subject of detection. In addition to contrast and noise level, detectability will depend on many factors such as: object features (size, shape, edge sharpness, etc.), background features (anatomical noise, noise texture, etc.), observer features (vision, experience, viewing distance, lighting conditions, screen luminance, etc.) [1, 34-36]. LCD is ultimately determined by human observers but since this task is time consuming and observer dependent, various computer-based methods have been developed. These range from simple methods that are more suitable for quality control, such as merely analyzing the variance in an image to predict LCD based on assumptions [1], to much more sophisticated techniques suitable for optimization and detection studies, like the so-called model-observers [37]. The model-observers are designed to mimic the detection performance of human observers, allowing comparisons of many combinations of scan- and reconstruction parameters, resulting in large amounts of images that would be unfeasible for radiologists to classify manually. One additional benefit of using a model-observer is that the threshold for classifying an image as "object present"/"object absent" can be varied arbitrarily, meaning that the ROC-curve can be obtained (although note that it can be estimated via human observers too by classifying the images at several distinct confidence levels).

1.4.1.1 Contrast-to-Noise Ratio

Contrast-to-Noise Ratio (CNR) can be defined as

$$CNR = \frac{HU_{obj} - HU_{bg}}{\sigma_{bg}} \quad (11)$$

where HU_{obj} and HU_{bg} is the mean value of the object and background respectively (measured in Hounsfield units) and σ_{bg} is the standard deviation of the background (measured in Hounsfield units). If all else is equal (i.e. the factors mentioned in section 1.4.1 above), the LCD should be maintained when the CNR is constant. However, that may often not be the case. One of the most important pitfalls of the CNR method is that noise (as measured by the standard deviation) is not necessarily sufficient, since it does not capture the texture of the noise which is very important for LCD. In particular, coarse noise has a negative impact on LCD since it obscures the object boundaries as compared to a fine-grained uncorrelated noise. The so-called noise power spectrum (NPS) is an alternative measure of noise which is more informative than the standard deviation. The NPS contains information about the level of variance for each spatial frequency, with lower frequencies corresponding to higher granularity. In recent years, iterative reconstruction algorithms have been given much attention as they have been widely introduced in clinical routine. These algorithms have an especially strong tendency to left-shift NPS (i.e. increasing the granularity of the noise), which can degrade LCD even though the standard deviation is equal.

1.4.2 Spatial Resolution

Spatial resolution (also called high-contrast resolution) is the system's ability to separate high-contrast details. Since resolution cannot easily be assessed by the visibility of a single small object (a blurred version of the object would always be visible given a high enough contrast), it is instead specified in terms of line-pairs per cm (lp/cm). This is most straight-forwardly tested by imaging a phantom containing high-contrast bar test patterns. Because of the system's blurring, a contrast loss occurs between the bars and the equally wide spacing between the bars, which increases as lines get thinner. Below 10% contrast it is difficult for observers to discern the bars from the spacings, hence the lp/cm at this contrast level is often called the limiting spatial resolution (and explicitly determined in quantitative methods). The most common automatic technique to assess resolution is to calculate the so-called modulation transfer function (MTF), which is typically done via Fourier transform of a point spread function (PSF) or line-spread function, acquired by scanning a dense thin wire, bead or edge. The PSF is the system's response to a point object (delta-function), and hence contains information over a range of spatial frequencies. The MTF's value for a given frequency (lp/cm) indicates how much the signal has been modulated down compared to a 100% contrast case, i.e. the MTF provides a measure of how well the system transfers contrast for different spatial frequencies.

Several factors affect spatial resolution. The most important for in-plane resolution are focal spot size, detector element size, number of projections and convolution kernel, while longitudinal resolution is dominated by slice thickness.

In an optimization context, it should be noted that spatial resolution is only weakly affected by image noise, since the contrast in question is typically high. This is illustrated in Figure 3,

which shows the MTF for different tube currents between 10–300 mAs. In this example, of a very high-contrast object, there was no decrease in resolution with decreased mAs (i.e. increased noise). In fact, the MTF-curves for the higher mAs-acquisitions are slightly lower and a marked drop is seen at 300 mAs (600 mA), likely attributable to focal spot blooming which increases with higher tube currents.

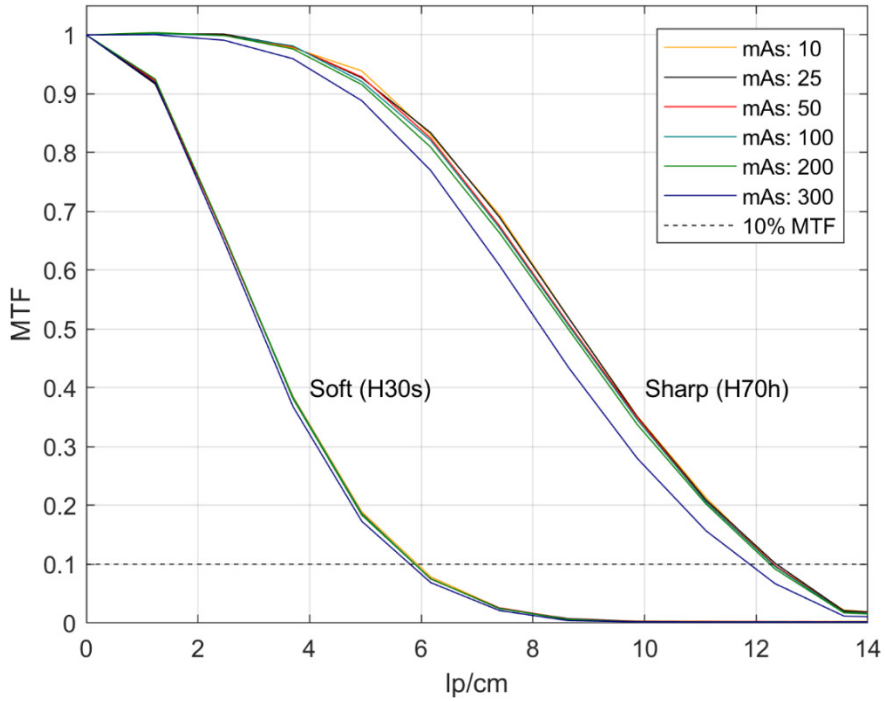

FIGURE 3: MTF curves for different tube currents between 10–300 mAs using a soft (H30s)- and sharp (H70h) convolution kernel. The images were acquired on a Siemens Biograph Edge, using 120 kV with a rotation time of 0.5 s; and the curves were calculated via the point-spread-function of a thin metal wire in a plastic phantom orthogonal to the scanning plane, using the mean MTF-curve from three consecutive 4.8 mm slices.

1.5 OPTIMIZATION TECHNIQUES

Many innovations and technical approaches have been used to optimize radiation dose and image quality in CT examinations. Among the most noteworthy is automatic tube-current modulation (ATCM), and more recently: x-ray spectrum optimization and iterative reconstruction algorithms. Iterative reconstruction will not be discussed further in this thesis in any detail, but the current status has been comprehensively summarized elsewhere [38].

1.5.1 Automatic Tube-Current Modulation

One of the most important inventions to reduce radiation dose in CT is the automatic tube-current modulation (ATCM) [3]. In earlier CT practice, the tube current was kept constant throughout the scan. But since differences in x-ray attenuation between lateral and anterior-posterior directions are often orders of magnitude (because of the exponential relationship

between distance and attenuation), and since the final noise levels of the image are dominated by the noisiest projections, it was realized that the tube current could be reduced at certain x-ray tube orientations without significant effects on image quality. Total radiation dose savings throughout the body have been reported to be in the range of 15%–53% for various body parts [3]. In addition to angular modulation, all scanners produced nowadays use longitudinal modulation (z-modulation) in combination with angular modulation. The purpose of the longitudinal modulation is to reduce the noise variations in the longitudinal direction, although it does offer some additional dose reduction [3].

Because the ATCM is almost always used, it is an integral part of most CT protocol optimization. One important part of the ATCM is the so-called localizer image. A localizer image is a planar projection of the patient that is taken before the diagnostic scan. It is acquired by having the x-ray tube and detector in a static position while the table is moving, allowing for the generation of projections of arbitrary length. The localizer image is used by the radiographer to get an overview of the patient's anatomy which is used to define the scan range, check for metal or other objects that can cause artifacts, verify patient positions, etc. The localizer image is also used by the ATCM to estimate the patient's attenuation, in order to modulate the tube current accordingly (see Figure 4). The acquisition technique used for the localizer, especially the orientation, can have very large effects on the ATCM [39]. This has largely been overlooked, until recently, when it has received increased attention [40-42].

FIGURE 4: Left and middle image: lateral- and posterior-anterior localizer respectively. Right image: a frontal projection made from the axial slices in the subsequent scan by simple summation of CT-numbers along the y-plane. The superimposed red curve indicates the effective mAs (defined as mAs÷pitch; which is proportional to the radiation dose) that was used in each slice. The curve has a characteristic increase in the shoulders and hips, with a decrease in the lung region. Note that the curve is the mean value each position, meaning that the total variation in tube current is larger than indicated by the graph since the angular variation is not seen.

1.5.2 X-ray Spectrum Optimization

In balancing radiation dose, CM dose and image quality, the most important tool is likely x-ray spectrum optimization [3, 43, 44]. It has historically been the norm to use a tube voltage of 120 kV for all types of examinations. However, in recent years, there has been a large upswing in task specific x-ray spectrum optimization, facilitated in large by the development of more powerful generators and better tube cooling, allowing both lower peak tube voltages and/or high levels of beam filtration.

1.5.2.1 Dose-Weighted Contrast-to-Noise Ratio

Because CNR increases with radiation dose (since the quantum noise will decrease), this parameter alone is not sufficient to optimize imaging protocols. The essential question one often wants to answer is "which settings allows for the lowest radiation dose, for a given CNR necessary for the imaging task?". The dose-weighted contrast-to-noise ratio (CNRD) is a better figure-of-merit to answer that question. CNRD is defined as

$$CNRD = \frac{CNR}{\sqrt{Dose}} = \frac{HU_{obj} - HU_{bg}}{\sigma_{bg}\sqrt{Dose}} \quad (12)$$

where HU_{obj} and HU_{bg} is the mean value of the object and background respectively (measured in Hounsfield units), σ_{bg} is the standard deviation of the background (measured in Hounsfield units) and *Dose* is the radiation dose (typically $CTDI_{vol}$). Because the radiation dose enters the formula as its square root value, CNRD will be independent of the actual mAs-value used (under normal conditions), since the factor $\sigma_{bg}\sqrt{Dose}$ is constant (noise decreases/increases in proportion to the square root of the radiation dose). CNRD will depend primarily on object properties (Z and density), x-ray spectra (kV, filtration and detection efficiency) and patient properties (size, shape and compositions). For instance, while lowering the kV will increase contrast in materials of different Z-values, x-ray penetration will drop resulting in higher noise levels for a given dose. E.g.: the optimal tube voltage for imaging a slim patient when only considering iodine CNR can be as low as 50 kV, whereas the optimal tube voltage for a large patient when considering only pure density differences might be >140 kV [45]. Optimal in this case means yielding a specific CNR at the lowest radiation dose (i.e. highest CNRD).

2 AIMS

Study I	The aim of this study was to evaluate the potential of low-kV dual-source (DS) and dual-energy (DE) to reduce CM-doses while maintaining soft-tissue and iodine CNR in phantoms of varying size, and to quantify the corresponding radiation dose increases.
Study II	The aim of this study was to implement and evaluate a scanning regimen, based on the results from Study I, to reduce CM-doses for patients believed to be at risk of CIN.
Study III	The aim of this study was to compare the outcome in image noise and radiation dose in the subsequent CT scan following a single anterior-posterior (AP) versus a combined lateral plus AP (LAT+AP) localizer when using automatic tube-current modulation (ATCM).
Study IV	The aim of this study was to evaluate if standard-dose CT can be replaced with low-dose CT for characterization of non-specific findings in bone scintigraphy.

3 MATERIALS AND METHODS

3.1 EQUIPMENT

3.1.1 CT Techniques

In Study I and II a 64-slice Somatom Definition Flash (Siemens Healthineers, Forchheim, Germany) was used in both single-source (SS), dual-source (DS) and dual-energy (DE) mode. In DS mode, two x-ray tubes and detectors at about 90 degrees angle are used simultaneously (Figure 5). The reason for this design is threefold: higher available total output (e.g. obese protocols), faster available speeds (e.g. heart- or pediatric protocols) and the potential of DE acquisitions (by using two different tube voltages, see Figure 1).

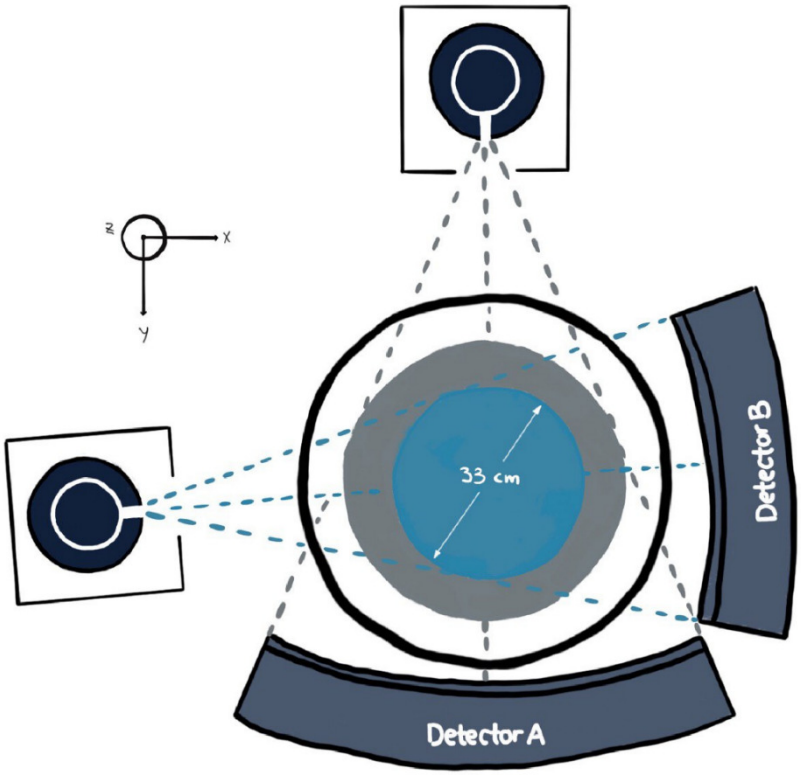

FIGURE 5: Schematic drawing of a Somatom Definition Flash dual-source scanner. The three concentric circles correspond to (from inner to outer) the scanned field of view of system B and A (33 and 50 cm respectively) and the gantry opening (78 cm). The drawing is not to scale.

The system is equipped with a software called Care kV, which based on the localizer data and indicated tissue of interest (slider position) selects the estimated optimal kV for the scan. This function in based on the use of CNRD as a figure-of-merit (described in section 1.5.2.1). In Study I and II Care kV was used in semi-mode. When used in this mode the user selects

the kV and the system then adjusts the mAs, based on a reference kV, reference mAs and slider position, to maintain noise levels similar to that of the reference. By adjusting the slider position, the noise level can be controlled in steps from higher to lower, as compared to the reference. Using slider positions instead of mAs-steps was deemed practical, and therefore used in Study I and II. It has the further advantage that the exposure parameters can be reported in terms of reference kV, reference mAs, used kV and slider position, meaning that other sites would not need to translate the results via their current reference settings. Further, the system is equipped with a longitudinal and angular tube current modulation (ATCM) software called Care Dose 4D, which was used in all scans. Care Dose 4D uses the information from one or two localizer to prescribe the longitudinal tube current modulation, in combination with live feed-back from the detector during the scan to modulate in the angular direction. When using two localizers of different orientation, the information from both images is used.

Study III was also performed on a Somatom Definition Flash using standard SS mode only.

Study IV was performed on an Emotion 16-slice SPECT-CT scanner (Siemens Healthineers, Forchheim, Germany), also equipped with Care Dose 4D.

3.1.2 Phantoms

In Study I, four quasi-anthropomorphic abdominal phantoms (Tissue Equivalent CT Dose Phantoms, CIRS, Norfolk, VA) were used to simulate adult abdomens of sizes (AP×LAT cm) 18.5×24, 22×30, 25×32.5 and 31×38.9, corresponding to a body mass index (BMI) of approximately[7] 16, 23, 26 and 35 kg/m^2 respectively (Figure 6). These phantoms are made of proprietary epoxy that closely mimics the x-ray absorption and scatter properties in the diagnostic energy range. Each phantom includes an embedded vertebral bone equivalent rod, mimicking the spine, and five bore-holes for dose measurements at center and peripheral positions.

[7] Estimated via regression coefficients from Menke 2005 [46]. These estimates were successfully replicated (about 5% difference) by me in an unpublished work using a different method in a set of 41 patients collected for other purposes.

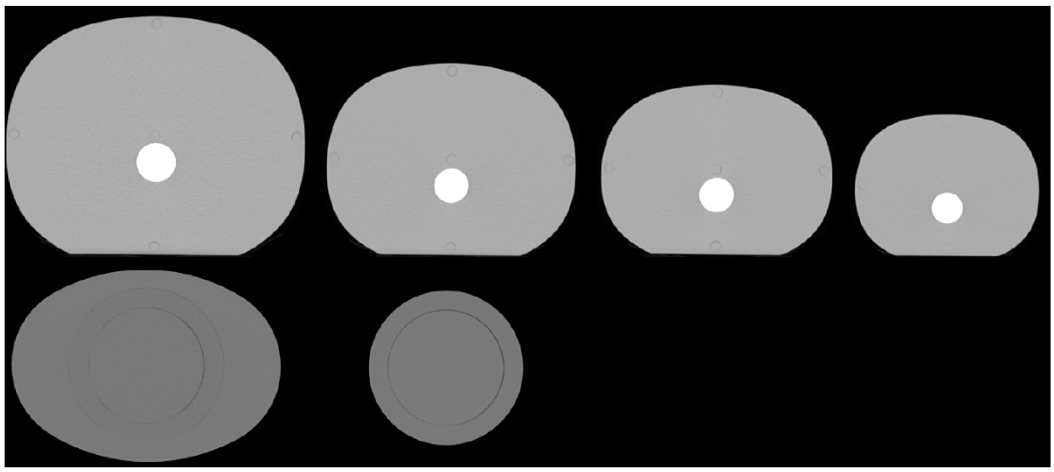

FIGURE 6: CT images of the CIRS phantoms (top row) and Catphan with and without extension (bottom row). The images have the same pixel size so that the relative sizes can be compared.

Additionally, a dedicated image quality phantom (Catphan® 600, the Phantom Laboratory, Salem, NY) was used. This phantom contains a low contrast module (module CTP515) consisting of a soft-tissue equivalent background with 39 inserted cylinders of varying sizes between 2–15 mm with nominal target contrast levels of 1%, 0.5% and 0.3%. The inserts have the same Z_{eff} as the background but deviate in density, which is an important property whenever a performance comparison involve different spectrums (e.g., different scanners or different kV-settings). The phantom was used without and with an oval extension ring of soft-tissue equivalent material (CTP579 25–30 cm OD oval annulus, the Phantom Laboratory, Salem, NY), corresponding to a BMI of about 28 kg/m^2 (Figure 6).

3.2 STUDY I & II

Five scan techniques: single-source 70 kV (SS70), dual-source 70 kV (DS70), single-source 80 kV (SS80), dual-source 80 kV (DS80) and dual-energy (DE), were compared to the reference 120 kV protocol to find CM-reductions and scan settings that would match both the iodine- and soft-tissue-CNR of the reference protocol for a wide range of abdominal sizes. This can be achieved in different ways. The approach opted for in this paper was to match the noise levels of the reference protocol (meaning that for non-enhancing soft tissue or other materials $CNR_{SS/DS/DE} \geq CNR_{120\,kV}$) while reducing CM the maximally allowed amount so that $contrast_{SS/DS/DE} = contrast_{120kV}$ (meaning that for iodine enhanced tissue $CNR_{SS/DS/DE} = CNR_{120\,kV}$). The four quasi-anthropomorphic phantoms (described in section 3.1.2 above) were used to simulate adults' abdomens with BMIs of approximately 16–35 kg/m^2. Syringes filled with CM-concentrations of 0, 2, 4 and 8 mgI/ml, that could be inserted into the phantoms, was prepared by dilution of 400 mgI/ml Iomeprol with saline. The noise and radiation dose levels where then assessed in 8 steps (slider position settings 1–8 for the SS/DS protocols, and 8 quality ref-mAs steps for the DE protocol), yielding 328 acquisitions (reference protocol × 4 phantoms × 2 repeats + 5 SS/DS/DE × 4 phantoms × 8 dose levels × 2 repeats), while the

contrast measurements were performed at one dose level only, yielding 192 acquisitions (4 concentrations × 6 protocols × 4 phantoms × 2 repeats). The CT-numbers in the syringe was measured in one 18 mm^2 region of interest (ROI), and image noise (defined as the standard deviation of the pixel values) was measured in two 30 cm^2 ROIs corresponding to the liver position. All measurements were averaged over three consecutive slices and two scans, and performed automatically using ImageJ and a purpose-written macro (ImageJ Version 1.46, National Institutes of Health, http://imagej.nih.gov/ij).

To find the CM reduction with maintained contrast, linear regression was performed to get the slope-coefficient, β (for CT numbers as a function of CM-concentration). The reductions could then be calculated as the ratio of β at 120 kV to that of the low-kV or DE protocol. The line of reasoning was that

$$Contrast_{kV} = Object_{kV} - Background_{kV}$$

$$Contrast_{kV} = (\beta_{kV} CM_{kV} + Bg_{kV}) - Bg_{kV} \tag{13}$$

where $\beta_{kV} CM_{kV}$ is the enhancing tissues' CT-number increase given a certain concentration CM_{kV}, and Bg_{kV} is the CT-number of the background (or more general: the non-enhancing tissue, since an object can be both hyper- or hypo-vascular). Because the aim was to maintain image contrast, i.e. that the contrast at 120 kV would be equal to the evaluated SS-, DS- and DE protocols, we get

$$Contrast_{120} = Contrast_{SS/DS/DE}$$

$$(\beta_{120} CM_{120} + Bg_{120}) - Bg_{120} = \left(\beta_{SS/DS/DE} CM_{SS/DS/DE} + Bg_{SS/DS/DE}\right) - Bg_{SS/DS/DE}$$

$$\frac{CM_{SS/DS/DE}}{CM_{120}} = \frac{\beta_{120}}{\beta_{SS/DS/DE}} \tag{14}$$

meaning that the ratio of CM-concentration can be determined by the ratio of the β-coefficients.

Although the reconstruction kernels were the same in the evaluated protocols, both the DS and DE protocols have additional pre-processing steps such as scatter correction. It was unclear if this could alter the noise texture and hence invalidate the CNR method. For this reason, an additional LCD assessment was performed, using the low contrast module of an image quality phantom (Catphan® 600, the Phantom Laboratory). Two blinded readers rated the detectability of each object on a four-point scale, where 4 = *clearly visible with distinct margins*, 3 = *clearly visible with indistinct margins*, 2 = *Vaguely visible*, and 1 = *Not visible*. A consistent LCD and matched CNR for the compared protocols were assumed to indicate comparable image quality.

The statistical analysis in the study consisted of an analysis of covariance (ANCOVA) to assess differences between β-coefficients, using the factor scan-setting, covariate CM-concentration and the interaction scan-setting × CM-concentration, where the interaction tests the null-hypothesis that the slopes are equal. The Mann-Whitney U test was used to test if

there were differences in LCD.

Based on the results of Study I, four low-kV scan protocols with specific settings (SS70, DS70, SS80 and DS80 selected based on patient size) for reduction of CM dose was implemented in clinical use and evaluated. The experimental group, which consisted of 43 patients older than 60 years with a reduced kidney function, defined as an estimated glomerular filtration rate (eGFR)<45mL/min, were scanned prospectively with a reduced iodine CM dose of 0.25 or 0.3 g/kg, depending on protocol. The control group consisted of 43 retrospectively included consecutive patients scanned during the same period, aged > 60 years with an eGFR>45mL/min using the routine abdominal 120 kV protocol and a CM dose of 0.5 g/kg. Imaging was performed in the portal-venous phase using a threshold value of 160 HU plus 45 s scanning delay with an injection duration of 30 s for both groups.

Measurements of liver CT numbers and noise was performed in threes slices (approximately 3 cm caudal of the hemi diaphragm; at the liver hilum; and approximately 3 cm cranial to the caudal edge of the liver), using a circular ROI with a diameter of 10–20 mm. Muscle CT numbers and noise were measured at the same three positions in the right erector spinae muscle, with a 5–10 mm diameter ROI. The main outcome variables were liver CNR and muscle- and liver noise. The muscle CT numbers was used as a surrogate for the background value in the CNR calculation. All CT numbers and noise measurements were performed by two independent readers and averaged for each ROI-position. SSDEs was calculated based on D_{eff}-measurements performed at the position of the kidneys using equations 7 and 8.

Statistical analysis was performed to assess differences in mean values using an independent t-test, where the normality assumption for the sample distribution of the means was considered fulfilled due to the sample size (n > 30). All p-values were corrected for multiple testing using the Benjamini and Hochberg method. 95% confidence intervals (CI) for the main outcome variables was calculated using a one sample t-test. The reader agreement was assessed using intra class correlation coefficient (ICC; two-way mixed model for consistencies with the average measure coefficient as outcome). A post hoc power calculation, with a power of 0.8 and alpha of 0.05, was performed for two different example CNR effect sizes: 0.45 and 0.9. The first, smaller, effect size corresponds approximately to either a decrease in enhancement of 5 HU or a noise increase of 11%, while the second, larger, effect size corresponds approximately to either a decrease in enhancement of 10 HU or a 5 HU decrease combined with a noise increase of 12% (both cases assuming a reference contrast enhancement, noise and CNR standard deviation of 50 HU, 11 HU and 1.5 HU/HU respectively).

3.3 STUDY III

299 patients examined with the routine thorax protocol of the department were prospectively scanned using either a single AP- or a LAT+AP localizer. The groups were compared in terms of noise- and effective mAs (mAs_{eff}) consistency due to differences in

ATCM performance in the spiral scan following the localizers. The performance was analyzed by comparing normalized root mean squared error (nRMSE) for noise and mAs_{eff} as a function of patient size. Larger nRMSE indicate a higher variability and less consistent inter-patient noise and mAs_{eff} in clinical routine.

Image noise was measured at two positions in the liver parenchyma, and in two positions in the aorta in the thorax region, using two free-hand ROIs, avoiding conspicuous vessels in the liver and streak artifacts and stenosis in the aorta. Because of the high CT-numbers in the aorta, both a narrow- and wide window setting was used during ROI-placement since the artifacts are more easily seen with the narrow window while this setting can be insensitive to stenosis being included in the ROI (with both the stenosis and surrounding CM enhanced blood seen as white).

Patient D_w was automatically calculated in the same axial slice as the noise measurements via equation 9 and 10, using a purpose-written Matlab-script (MathWorks Inc., Natick, MA, USA). The D_w-script was validated using the four quasi-anthropomorphic phantoms (described in section 3.1.2). Because many patients had peripheral areas that were outside the reconstructed field of view D_w was not calculated in all cases. Therefore, complementary size measurements were performed in the localizer image in form of line profile sums (LPS), defined as the sum of the pixel-values across the patient width at the longitudinal position corresponding to the axial slice (found via the DICOM metadata). The relationship between LPS and D_w was then established using linear regression (on both groups, i.e. AP and LAT+AP combined), and subsequently used to impute missing D_w-values.

mAs_{eff} was collected from the DICOM metadata at the measurement position (it is defined as mAs÷pitch)

Statistical analysis was performed to assess differences in nRMSE between the groups for mAs_{eff} and noise as a function of D_w. Linear regression was carried out (after data transformation by $\ln(mAs_{eff})$ to produce a linear relationship). To find the 95% CI of the nRMSE, percentile bootstrapping was used with 3000 iterations and re-sampling with replacement. To test the null hypothesis (i.e. that there was no difference in nRMSE between the AP and LAT+AP groups) a distribution of nRMSE-differences was generated by taking the nRMSE for the AP group minus that of the LAT+AP group for each of the re-samples. If the 95% CI of this difference-distribution did not overlap zero, it was considered a statistically significant difference.

3.4 STUDY IV

During approximately an eight-month period, all oncological patients that were referred to the department[8] for bone scintigraph with 99mTC-HDP who met the inclusion criterion were asked to volunteer in the study. The inclusion criteria were: age > 60 years with two or more

[8] Nuclear Medicine, Karolinska University Hospital, Stockholm, Huddinge

focal uptakes in the lower spine and/or pelvis that after assessment of the bone scintigraphy was considered of unclear origin and in need of further radiological examination. Nineteen patients with a total of 50 uptakes were recruited. These patients were examined with a whole-body bone scintigraphy followed by the standard-dose CT (both standard procedure) directly followed by, without repositioning, an additional low-dose CT. The CT-protocols were identical (110 kV, 16×1.2 mm collimation, 1.5 pitch, 0.6 rotation time and a medium smooth reconstruction kernel B31s) except for quality reference mAs which was lowered from 89 to 17 in the low-dose protocol.

Two sets of images were prepared: bone scintigraphy paired with the standard-dose CT and another set paired with the low-dose CT. The images were anonymized and randomly divided into two lists for reading. Both lists contained all patients: either the standard-dose or low-dose of each patient in random order. Before the readings one reader viewed all bone-scintigraphy images and defined two or three positions of focal uptake. These predefined positions were then read by four experienced radiologists and rated as: 1 = *benign lesion*, 2 = *malignant lesion*, 3 = *no finding*, 4 = *do not know*. The order of rating was separated, so that two of the readers first rated the first list while the other two started with the second. To reduce the impact of recollection, a minimum of one month between two readings was allowed.

The main outcome analysis was to test for a shift in rating frequencies from the standard- to the low-dose CT, by use of the Stuart-Maxwell chi-squared test for marginal homogeneity. Additionally, the inter-observer agreement when using the standard- versus low-dose CT was compared by use of the Light's kappa value with 95% CIs, estimated by percentile bootstrapping. To test for differences between the Light's kappa values, a distribution of differences was generated through bootstrapping by taking the kappa value of the standard-dose minus the low-dose for each resample. If the 95% CIs of the difference-distribution did not overlap zero, this was considered significant. Finally, intra-observer agreements were quantified by use of the Cohen's kappa.

4 RESULTS

4.1 STUDY I & II

The phantom experiments showed that a 50%, 40% and 20% reduction of CM should be achievable with the 70 kV, 80 kV and DE-protocol respectively. As expected, the β-coefficients increased with decreasing tube voltage and decreased with increasing phantom size (due to beam hardening). There was a small (statistically significant; not clinically significant) difference in β-coefficients between the SS and DS protocols (likely due to minor differences in filtration). It was possible to match noise levels for all phantom sizes when using the DS80 kV and DE protocol (Figure 7).

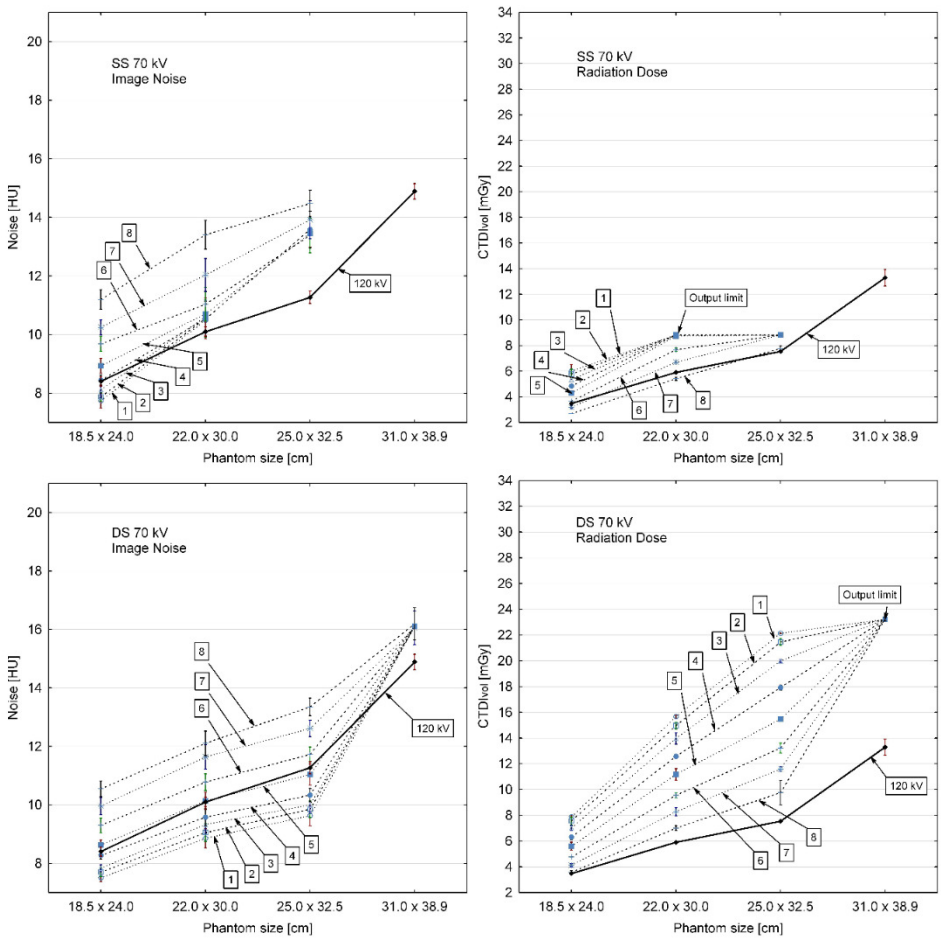

FIGURE 7: Noise and radiation dose data with corresponding 95% CI for the evaluated low-kV protocols (dotted lines) and the reference 120 kV protocol (solid line), for each phantom size. For the SS- and DS protocols, each of the eight slider positions are shown, whereas for the DE protocol only the lowest (320), highest (390) and best match (350) reference mAs settings are shown (next page).

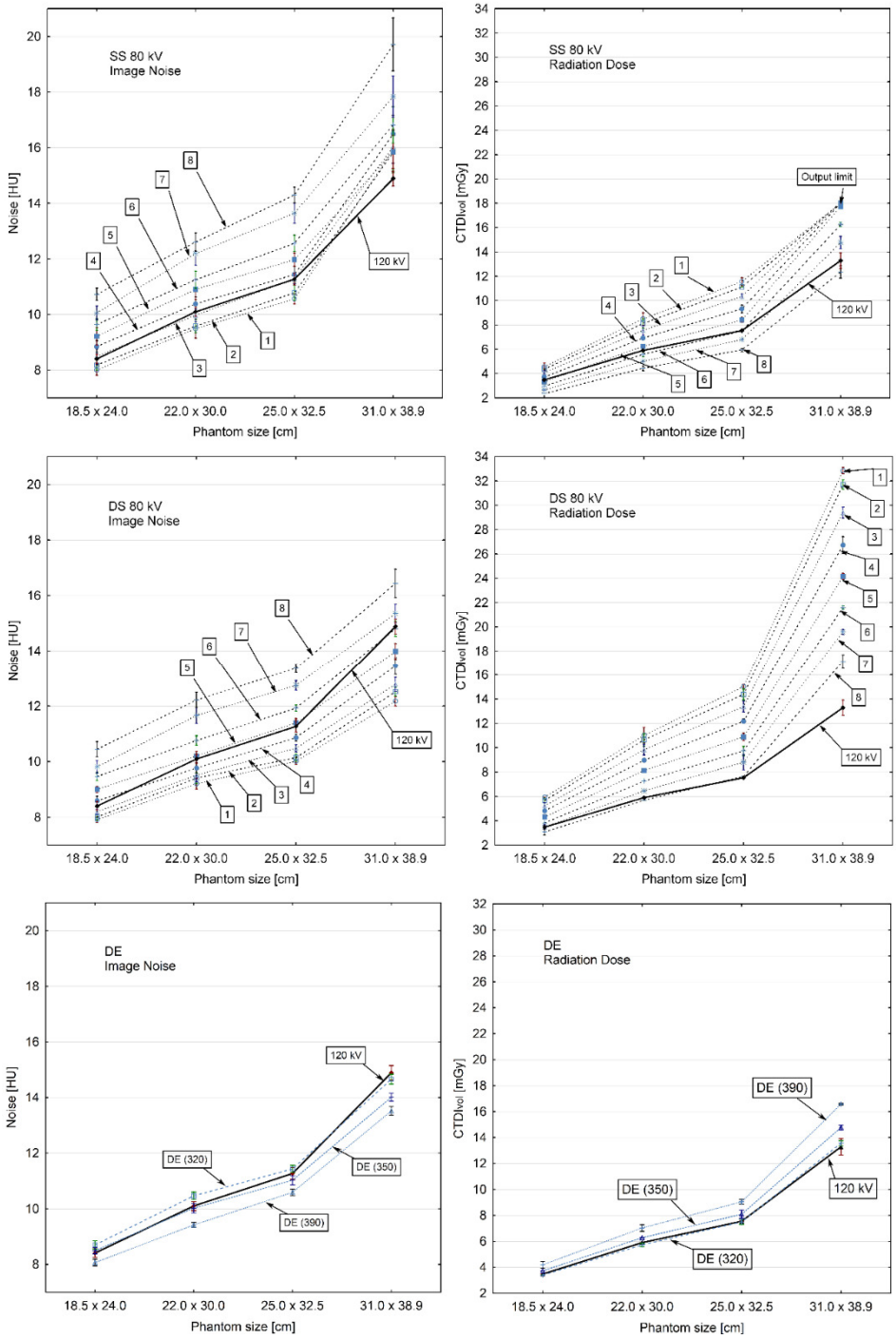

FIGURE 7: (Continued.)

There was no statistically significant difference in LCD between any of the protocols. Depending on phantom size, the radiation dose increase ranged between 23–107% for the DS protocols, 17–39% for the SS protocols and 6–12% for the DE protocol. Based on this, a table of scan protocols could be devised (Table 1) that matched both iodine- and soft tissue CNR, indicating the tradeoffs between CM reduction and radiation dose increase for all abdominal sizes.

TABLE 1: CM reduction and radiation dose increase for each protocol at maintained CNR. The low-kV and DE protocols are presented with the slider position and reference mAs that best matched the noise levels of the reference protocol for all phantom sizes.

	15-Year-Old 18.5 × 24 cm	Small Adult 22 × 30 cm	Medium Adult 25 × 32.5 cm	Large Adult 31 × 38.9 cm
		SS 120 kV		
Noise [HU]	8.4	10.1	11.3	14.9
CM reduction	0%	0%	0%	0%
$CTDI_{vol}$ [mGy]	3.5	5.9	7.5	13.2
$CTDI_{vol}$ increase	0%	0%	0%	0%
		SS 70 kV (slider position 4)		
Noise [HU]	8.5	-	-	-
CM reduction	51%	-	-	-
$CTDI_{vol}$ [mGy]	4.8	-	-	-
$CTDI_{vol}$ increase	37%	-	-	-
		DS 70 kV (slider position 5)		
Noise [HU]	8.6	10.1	11.0	-
CM reduction	53%	53%	53%	-
$CTDI_{vol}$ [mGy]	5.6	11.2	15.5	-
$CTDI_{vol}$ increase	60%	90%	107%	-
		SS 80 kV (slider position 3)		
Noise [HU]	8.5	10.0	11.3	-
CM reduction	40%	40%	40%	-
$CTDI_{vol}$ [mGy]	4.1	7.6	10.4	-
$CTDI_{vol}$ increase	17%	29%	39%	-
		DS 80 kV (slider position 5)		
Noise [HU]	9.0	10.2	11.4	14.0
CM reduction	44%	44%	44%	44%
$CTDI_{vol}$ [mGy]	4.3	8.1	10.9	24.2
$CTDI_{vol}$ increase	23%	37%	45%	83%
		DE (ref. mAs 350)		
Noise [HU]	8.5	10.0	11.0	14.0
CM reduction	20%	20%	20%	20%
$CTDI_{vol}$ [mGy]	3.7	6.3	8.1	14.8
$CTDI_{vol}$ increase	6%	6%	8%	12%

In the patient study (Study II), there was no statistically significant difference in the outcome measures CNR, liver- and muscle noise between the groups, which confirms the phantom results. Further, there was no statistically significant difference in patient body sizes, measured as the body weight and effective diameter between the groups, which is a necessary condition for the comparison. Of the 43 patients in the reduced CM-group, a total of 5, 8, 17 and 13 patients were scanned using the SS70, DS70, SS80 and DS80. Figure 8 shows the distribution of CNRs for each protocol compared to the reference 120 kV along with the distribution of BMIs for the various protocols.

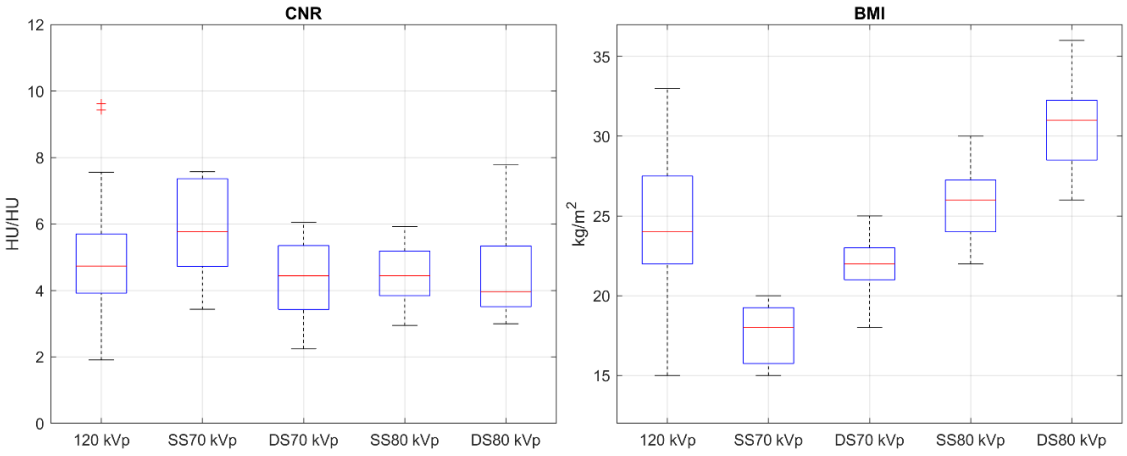

FIGURE 8: CNR and BMI distributions of patients scanned with each protocol.

The scan-times were longer for the low-kV protocols: about 13 and 28 seconds for the SS- and DS protocols, compared to 7 seconds for the 120 kV reference protocol. Radiation exposure, measured as the SSDE, was 70% higher on average for the low-kV group. The reader ICC was deemed excellent and good for the measurements of attenuation in the liver and muscle respectively, and moderate for the measurements of noise. The post hoc power calculation indicated a needed sample size (group size) of 172 and 44 for the two example CNR effect sizes.

4.2 STUDY III

Figure 9 shows mAs_{eff} and noise as a function of D_w, with the fitted functions. The LAT+AP group had a statistically significant lower nRMSE for mAs_{eff} and noise in the thorax region, and for noise but not mAs_{eff} in the liver region.

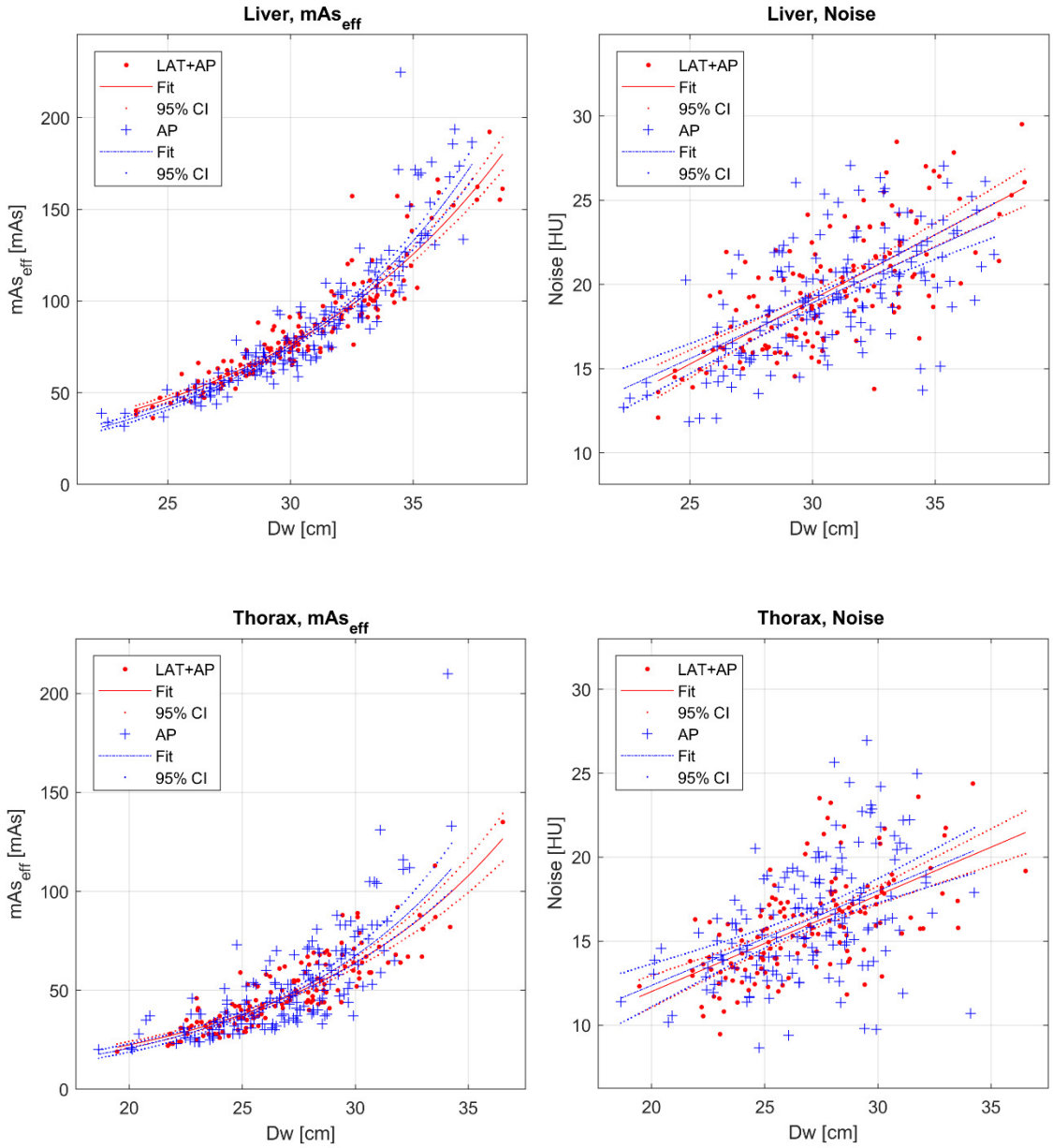

FIGURE 9: Effective mAs (left graphs) and noise (right graphs) as a function of D_w for both groups in the liver- (upper graphs) and thorax region (lower graphs).

A post hoc analysis was performed to assess the seeming fact that female patients with laterally protruding breast tissue was overrepresented amongst outlying cases. To analyze this, a script was written that randomly and blinded displayed an AP localizer from either group. The reader then selected whether the current patient had this characteristic anatomy or not, which is exemplified in Figure 10, resulting in a subset of 27 patients (18 AP and 9

LAT+AP), or about 20% of the females in the study. Figure 11 show the original data set with the subset indicated by circles.

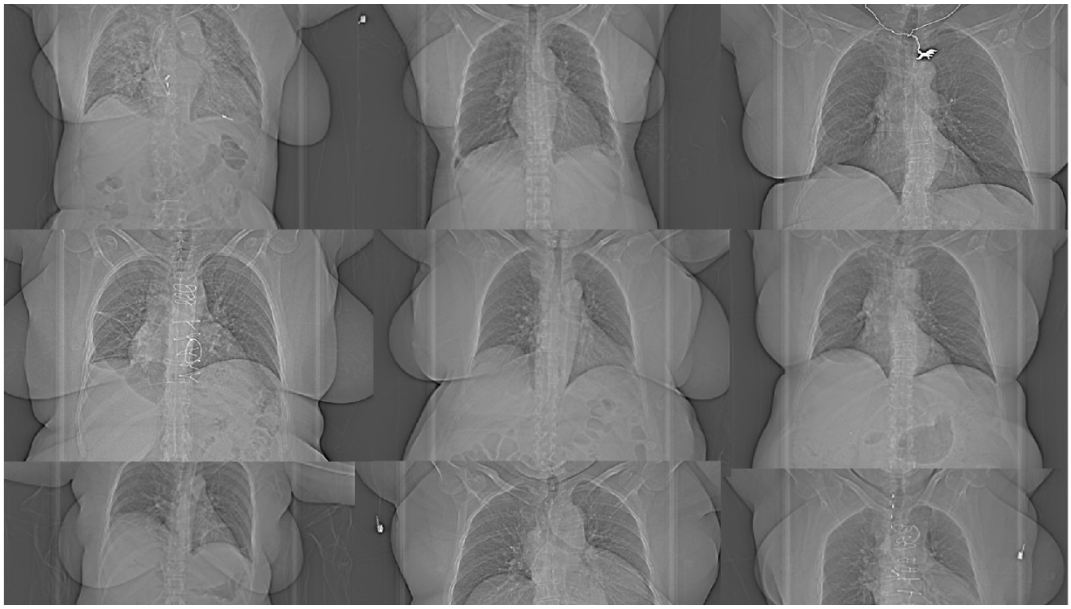

FIGURE 10: Examples of typical patients from the breast subset.

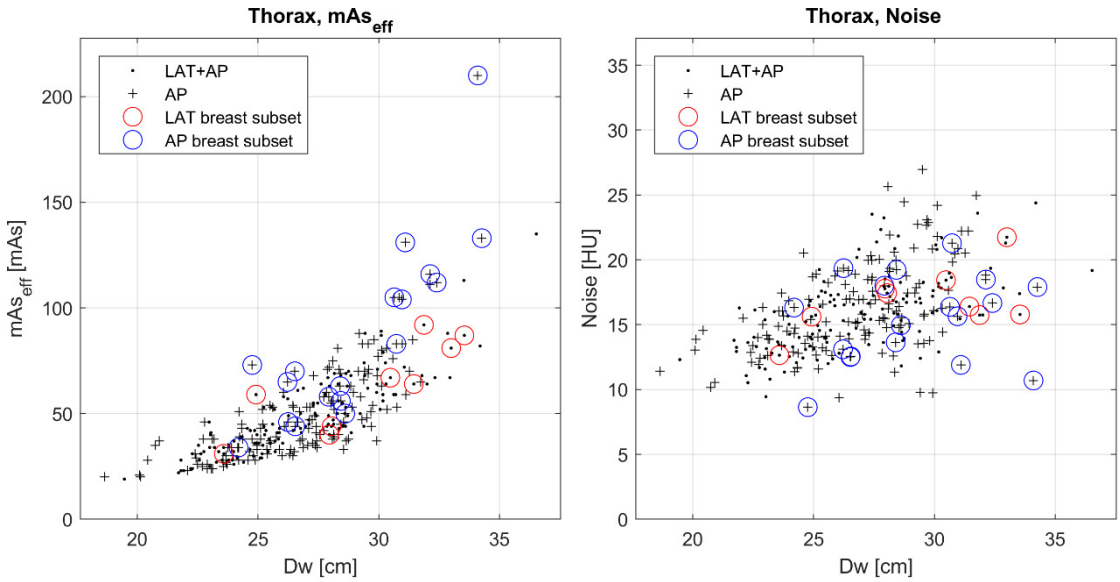

FIGURE 11: Effective mAs (left) and noise (right) as a function of D_w for both groups in the thorax region (same data as in Figure 1). Patients from the breast subset are indicated by circles.

The graph suggests that there is a particularly large difference between the AP and LAT+AP localizer for this subset of patients, with AP resulting in higher mAs_{eff} in combination with a lower noise than expected, which would mean that the higher mAs_{eff} was unwarranted. The mean noise level of the subset of the AP-group was 2.7 HU lower than expected (measured as the distance from the regression line for the non-breast-subset patients), corresponding to an estimated mean of about 57% higher radiation than needed for all individual cases to reach the expected noise. This deviance from the expected noise was analyzed statistically by

including a dummy variable as a second predictor (with dummy = 1 if the patient belonged to the breast subset, and dummy = 0 otherwise), resulting in the linear regression model: noise ~ 1 + D_w + dummy. The regression coefficient for the dummy variable was statistically significant in the AP case, but not for LAT+AP.

4.3 STUDY IV

The mean $CTDI_{vol}$ for the standard- and low-dose group was 5.8 and 1.2 mGy corresponding to an approximate effective dose of 4.2 and 0.8 mSv respectively. There were no statistically significant shifts in ratings between the standard- and low-dose protocol using the Stuart-Maxwell test for any of the readers (Table 2). There was no statistically significant difference in inter-observer agreements: Light's kappa values for the standard- and low-dose group were 0.68 (95% CI: 0.57–0.79) and 0.60 (95% CI: 0.47–0.72) respectively, with a difference of 0.08 (95% CI: -0.075–0.25). The intra-observer agreements were 0.77, 0.76, 0.65 and 0.68 (mean value 0.72) for the readers 1–4 respectively.

TABLE 2: All ratings for the paired standard- and low-dose images for each of the four raters. A value placed on the diagonal means that the same rating was made for both images. P-values refers to the Stuart-Maxwell test. (1 = benign, 2 = malignant, 3 = no finding, 4 = do not know.)

		Standard-dose			
Reader 1		1	2	3	4
Low-dose	1	17	0	1	0
	2	0	23	0	1
	3	1	0	1	0
	4	1	3	0	2

p=0.57

		Standard-dose			
Reader 2		1	2	3	4
Low-dose	1	20	0	1	0
	2	1	21	0	1
	3	0	0	2	0
	4	2	2	0	0

p=0.23

		Standard-dose			
Reader 3		1	2	3	4
Low-dose	1	16	1	0	2
	2	0	22	0	1
	3	0	0	0	2
	4	1	1	3	1

p=0.73

		Standard-dose			
Reader 4		1	2	3	4
Low-dose	1	21	0	1	0
	2	0	17	1	2
	3	1	3	2	0
	4	0	2	0	0

p=0.80

5 DISCUSSION

5.1 STUDY I & II

Previous studies investigating low-kV high-mAs techniques to reduce CM were limited to small and medium patients due to the output limitations of conventional CTs at that time. The work in Study I and II suggested and evaluated the use of DS technique to facilitate CM reduction in a wider range of patient sizes and included the use of 70 kV for further reduction, which to our knowledge had not been evaluated in previous publications. Additionally, previously published works focused on iodine CNR, while allowing noise levels to increase (sometimes in combination with adding iterative noise reduction to the low-kV protocol but not the reference; possibly violating the assumptions of the CNR method) which allowed reports of lowering both CM doses and radiation doses while maintaining CNR. For several types of examinations, like angiographic- and to some extent liver examinations, it may be reasonable to focus only on iodine CNR while allowing noise levels to increase. In the case of routine abdominal examinations however, soft tissue CNR requires consideration. With fat being the main exception, no image contrast improvement in general should be expected for soft tissue density differences when using a low tube voltage. In principal, this means that noise levels need to be kept constant in order to not reduce the CNR of non-enhancing tissue. Since the protocols evaluated in Study I and II are intended for use in routine abdominal examinations, the approach opted for was to match noise levels while reducing CM to the extent dictated by equation 14, which meant that radiation doses had to increase. More specifically, the radiation dose increased with decreasing tube voltage and increasing phantom size. This can be seen in Figure 12, where the normalized (to the reference protocol) dose-weighted contrast-to-noise-ratio (nCNRD) has been calculated for the evaluated protocols and phantom sizes. As seen in the figure, the low-kV protocols have a superior iodine CNRD compared to both the reference protocol and the DE protocol, while having an inferior CNRD for density differences. The DE protocol had better overall CNRD performance[9] compared to the reference protocol (similar for density, but higher for iodine) but it had a poor iodine CNRD as compared to the 70- and 80 kV protocols, making it unsuitable for the intended purposes. Further, as seen in the right-hand plot of Figure 12, the SS protocols have a higher measured CNRD for density differences than the DS protocols (except in the large phantom).

[9] Note that this is not to suggest that the DE protocol is a better choice for routine abdominal examinations. As per later non-published work, the DE protocol with mixed images has similar iodine CNRD as a single-source 100 kV protocol, while suffering from other disadvantages such as FOV limitations and longer scan times.

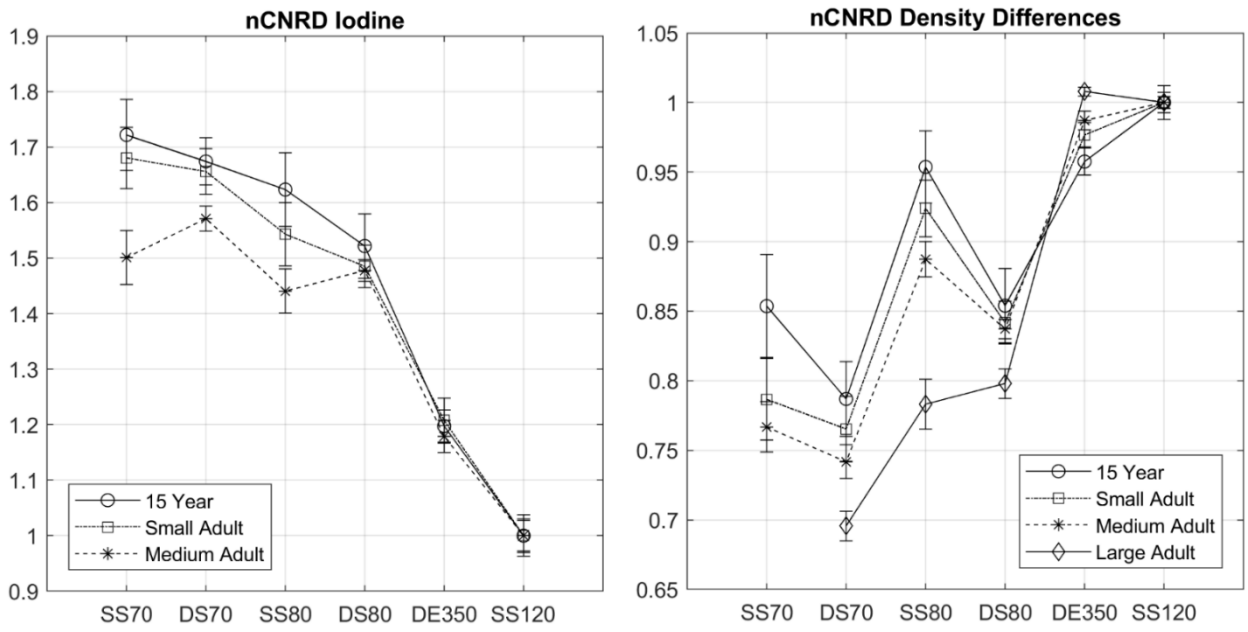

FIGURE 12: Dose-weighted contrast-to-noise ratios (CNRD) normalized to the 120-kV reference protocol (error bars indicate the error-propagated standard deviation). Left figure: normalized CNRD for the iodine measurements using the mean result from the three concentrations. Right figure: normalized CNRD for an example case of pure density differences, i.e. assuming no contrast improvement with decreased x-ray energy. Note that because the radiation dose enters the formula as the square root, a CNRD ratio of 1.7 means that the 120 kV protocol would need about a tripling of radiation dose to match the iodine CNR of the SS70 protocol in the smallest phantom (left figure), while a factor 0.7 indicates that the DS70 protocol would need to double the radiation dose to match the density CNR of the 120 kV protocol in the largest phantom (right figure).

This should be expected since in principle several factors make the DS protocols less dose efficient: slightly less beam filtering, more relative over-beaming, scatter between the two tube-detector systems, and two separate data acquisition systems. A further advantage of the SS protocols compare to the DS protocols was the shorter scan times (because of the wider collimation and therefore higher table feed). For these reasons, all four protocols were used in the patient study in order to utilize the advantages of the SS protocols when possible, so that, based on size, the protocols were selected in the order SS70→DS70→SS80→DS80. For practical purposes, however, BMI-ranges (based on the phantom study but updated based on clinical experience) for when to select a specific protocol was defined in the radiographer document, with the additional instruction to escalate the patient to higher scan protocol if the scanner indicated that the tube output limit would be reached at any location throughout the scan (typically the hips). Note that this method is likely sub-optimal since it means that no patients were de-escalated to a lower protocol, and hence would have saved either radiation- or CM dose. An alternative method of loading every protocol (from bottom to the top) in order to use the first one without output limitations, appears simple enough that it should be considered for adoption in the clinic.

The results from the patient study were in good agreement with the phantom experiments. Both iodine CNR and noise levels, as intended, were maintained for each protocol. Radiation exposure, measured as the SSDE, was 70% higher on average for the low-kV group, which is

in line with the phantom results[10].

A fixed CM injection duration of 30 seconds was used for both groups (i.e. injection rate was varied to compensate for varying injected volume). A fixed injection duration should yield equal shape of the enhancement curves [47], while the magnitude is scaled by the total dose. A chaser of saline with a volume of 50 ml was added to both groups, meaning that the ratio of saline to iodine differed. It is unclear whether this should have any effect on the shape of the enhancement curve, although it seems unlikely. If there is an effect, however, it should be small and apply only to arterial phase since parenchymal enhancement in the venous phase is principally determined by the total injected dose [48].

The most important limitation of Study I and II is that the patient study did not assess other aspects of image quality in addition to the quantitatively measures used. Instead, the patient study was a validation and further proof of concept of the phantom results. This was valuable, but the material could have been made more use of by adding some additional assessments for which phantom studies are unsuitable. Another limitation is that the LCD comparison in the phantom study was not adequately performed: lacking a sample size calculation and using a suboptimal method.

5.2 STUDY III

Almost all diagnostic CT imaging today is performed using some form of ATCM technique. The purpose of the ATCM is to adjust the x-ray exposure to the patient attenuation to reduce radiation dose and keep intra- and inter-patient image quality consistent. To our knowledge, no study has investigated the effect of localizer technique on inter-patient consistency. This study indicated a higher ATCM consistency when using LAT+AP than a single AP, but the difference was small except in the thorax region for the subgroup of females with laterally protruding breast tissue. This main outcome is not surprising since the ATCM-software has access to more attenuation information when using an additional LAT localizer, and is then much less susceptible to magnification effects from miscentering. The reason for the particular large difference for the breast group is likely due to the complex and irregular shape. The exact mechanism is difficult to specify due to the proprietary nature of the Care Dose 4D software, but it is clear from earlier phantom experiments that the software can react to unexpected geometries in a way that is not consistent with the actual attenuation values. In private communications with Siemens in connection to the phantom experiments they have stated that it uses sophisticated functions, which could perhaps be pattern- or image recognition features that are unfit for this special case. As seen from the AP point of view, these specific anatomical regions contribute a lot to the total width but far less to the total

[10] Although note that the mean size of each low-kV group represents a subgroup of sizes, hence it is necessary to stratify the 120-kV group into size-matching control groups, which was not done in the paper. Doing so yields about 30%, 80%, 45% and 100% increase for the SS70, DS70, SS80 and DS80 protocols respectively, which is well in line with the values in Table 1.

attenuation, so it might be a case of the algorithm placing to much weight on the former resulting in an overestimation of needed exposure, although this is only speculation. However, given that the finding was post hoc and, additionally, with a low number of observations, it should be replicated before drawing firm conclusions.

The main limitation of this study is that D_w does not take shape into account, specifically not the lateral width which typically dominates image noise formation, meaning that a given numerical value of D_w can result in a different mAs_{eff} if the shape is different. This point was shown by Burton and Szczykutowicz [49] using an ATCM from a different manufacturer. However, I replicated the finding using the Caredose 4D software (Figure 13).

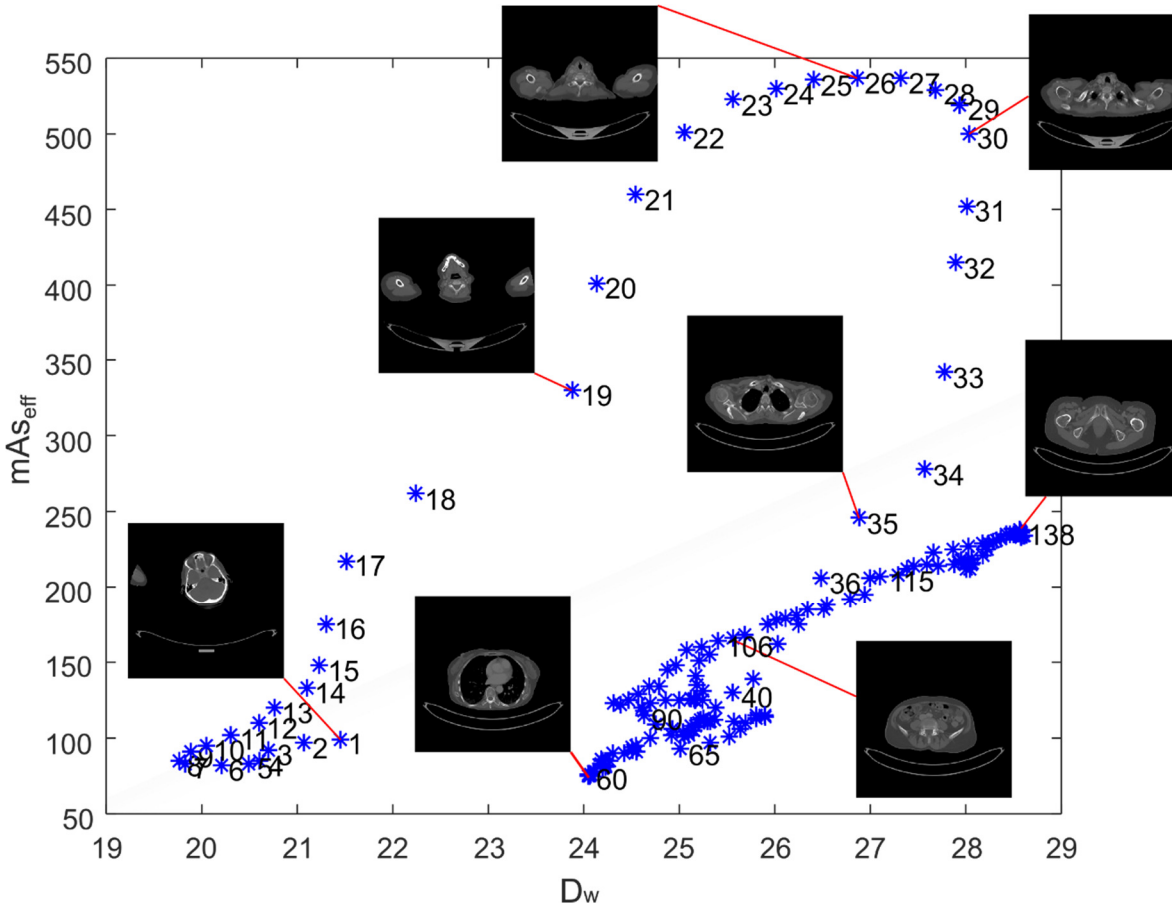

FIGURE 13: Shows the mAs_{eff} as a function of D_w through the body from the head to the pelvic region, in steps of 5 mm (acquired on a Siemens Edge with Care Dose 4D using a LAT+AP localizer). Evidently, the correlation between D_w and mAs_{eff} brakes down as ellipticity changes. For example: slice 30 (shoulders) has a slightly smaller D_w compared to 138 (hips) but more than a factor of two higher mAs_{eff}. For these slices the LAT/AP-ratio was about 3.5 versus 2.0, with slice 30 having over two half-value layers more tissue in the LAT direction. In this example however, there were local regions with little change in shape that showed very high correlation: the thorax region (excluding the apex/shoulder region) slice 40–60 and the hip region 106–138 both had a R^2>0.95.

This could be problematic for the study design because, even though the shape in the thorax- and liver position can be assumed to be similar on average for both groups, the larger range of mAs_{eff} values of the AP-group could plausibly be interpreted as the ATCM being more responsive to changes in shape not captured by the D_w-measurement. However, this

interpretation seems unlikely since all observed patterns remain when plotting mAs_{eff} and noise against lateral diameter (measured in the axial image) or LPS (measured in the AP localizer, i.e. in the LAT direction). Further limitations in the study relate to: the use of a high pitch value which has an obscuring effect on noise consistency differences due to higher inter-slice noise variations; the lack of a separate full-FOV reconstruction for D_w-calculations, resulting in the decision to impute cropped patients via the LPS; and the difference in table height adjustment frequencies between the groups, although this bias was estimated to be small.

There are pros and cons in using two localizers. The pros are that adding the LAT localizer allows for verification of patient centering, helps the radiographer to make a more precise prescription of scan length, and (as suggested by these results) increases consistency in image noise and mAs_{eff}. The cons are the added dose from an additional localizer and a minimal increase in examination time. In this case however, the added dose from the additional LAT localizer may be balanced by the dose savings in the CT scan. The estimated value of overexposure in the breast sub group (57% higher mAs_{eff}) was calculated to correspond roughly to an effective dose increase of 3 mSv (assuming a 10 cm region of the breast using a typical chest $CTDI_{vol}$). Since this applied to 10% of patients (20% of females), the population exposure increase would be about 0.3 mSv on average per examination, which is about the same as the dose from a typical lateral localizer (0.2 mSv).

The method suggested in this work could be improved based on the identified limitations, and implemented in a larger study including all vendors, which could be useful for the imaging community.

5.3 STUDY IV

The literature review of the article focused primarily on the field of nuclear medicine, in which little useful prior work was found. However, several previous studies have evaluated the use of low-dose CT for imaging of lumbar and facet joint disease and whole-body myeloma examinations. One study found no difference in sensitivity and specificity for lumbar examinations between a protocol with a $CTDI_{vol}$ of 7 mGy compared to 1.7 mGy using the consensus from MRI as reference [50]. Another study found low-dose CT at about 2 mGy superior to radiographic images at the same effective dose, using the European guidelines for CT and radiographic image quality criteria with a five-grade scale [51]. One especially informative study [52] for assessing the lower limits of radiation dose in assessing normal osseous structures (which in retrospect would have been useful at the time of writing the article) is from the field of myeloma imaging. In that study, the authors scanned a cadaver (above average size) using the most relevant combinations of scan parameters and the relevant dose-range of about 0.7–4 mGy and rated the image quality for various body parts using Likert scales. Both the 140 kV and 100 kV protocol at 1.1 and 0.72 mGy, respectively, were rated in the region of “average and/or diagnostic image quality” (which need to be interpreted in the context of the imaging task).

The scan parameters in the present study (110 kV, 1.2 mGy), however, were not informed by previous published work, but rather on a pilot phantom study (inspired by the experience of one of the authors who sometimes used the attenuation CT, which has about 30–40% lower dose than the low-dose protocol in the study). The study design differed from previous works in that it did not use any quantitative or qualitative measurements of image quality. Instead, it compared the diagnostic outcome in paired standard- and low-dose images of the same scintigraphy findings. One benefit of this design is that it directly assesses the metric that matters (i.e. there is no need to make a judgement call, based on an observed reduction in image quality, as to whether this reduction matter for diagnostic outcome or not). The drawback is that the results are very specific to the diagnostic task at hand. In this study, the rating system was tailored to be useful for the type of decisions that apply to such bone scintigraphy findings, which results in a study with less wide applicability as compared to some more general rating of image quality or diagnostic confidence using, say, the European guidelines quality criteria.

One way to assist interpretation of the data was to compare the standard- versus low dose results to the inter-reader results using only the standard dose. Table 3 (left matrix) shows the frequency of ratings for the standard- versus the low-dose case after summing the ratings for all four readers (i.e. 200 ratings).

TABLE 3: Left: the sum of all four reader's ratings from Table 2. Right: the sum of the inter-reader matrixes of the standard-dose images. P-values refers to the Stuart-Maxwell test. (1 = benign, 2 = malignant, 3 = no finding, 4 = do not know.)

Sum: reader 1–4		Standard-dose 1	2	3	4
Low-dose	1	74	1	3	2
	2	1	83	1	5
	3	2	3	5	2
	4	4	8	3	3
					p=0.62

Sum: inter-observer (standard-dose)		Reader x 1	2	3	4
Reader y	1	70	3	3	4
	2	3	85	4	7
	3	1	2	5	1
	4	8	1	1	1
					p=0.33

An exact correspondence would mean that every number was placed on the diagonal. Randomly scattered values above and below the diagonal implies lower reliability, whereas an overrepresentation of number either above or below the diagonal means a shift in ratings. As seen, there are 35 instances of mismatched ratings between the standard- and low dose ratings, with a greater number below the diagonal (21 vs 14; although note that the likelihood of getting a discrepancy ≥ 7 (21 minus 14) for 35 mismatches randomly distributed on either side is about 30%, calculated using a binomial distribution). For comparison, an inter-observer matrix (Table 3 right side) was generated by summing up all combinations of readers-vs-reader-matrixes (i.e. R1 vs R2, R1 vs R3 … R3 vs R4). Because there were six combinations of reader pairs, the numbers were scaled by a factor of 2/3 to make it comparable with the standard- vs low-dose matrix. There was a total of 38 mismatches in the comparison inter-observer matrix (22 above and 16 below the diagonal), which is very similar the intra-observer case. This is also reflected in the fact that the intra-observer agreement (i.e. same reader: standard- vs low-dose) was 0.72 on average, while the inter-observer agreement (using only the standard dose) was 0.68. These comparisons suggest that

that there is no indication that the discrepancies introduced by low-dose imaging are appreciably larger than that introduced by having a different reader. One improvement to the study would have been to include an intra-observer assessment for the standard-dose images to compare with the intra-observer for standard- vs low-dose (ideally performing the entire reading scheme twice, not just an extra standard-dose reading, so that one could control for increased recollection).

The major limitations of the study was the small sample size and that no sample size calculation was performed; and the problem of whether the observations should be treated as independent or dependent. The latter limitation is discussed at length in the paper, but the former warrants some further discussion. Since a null-result can be interpreted both as no effect, or that the sample was too small to detect the effect, the results are hard to interpret. Performing a sample size calculation for this rather unconventional analysis method would have been demanding but seems feasible. The crux would probably have been on the medical side: deciding how much of a shift, and from which categories, to deem as clinically acceptable not to detect. This would also have implied thinking about the cost- benefit situation (i.e. risk of misdiagnosis versus radiation risk) and the fact that the benefits of dose reduction for this particular patient category (average age 74 years; and with high prevalence of cancer) is very low. Although, the results could possibly have implications for other kinds of bony pathologies like joint arthritis, fractures and osteomyelitis.

6 CONCLUSIONS

Study I	In this phantom study, low-kV dual-source imaging could be used to reduce CM doses by 44–53% with maintained iodine-, soft tissue- and other materials CNR in a wide range of abdominal sizes, to the cost of about 20–100% increased radiation dose, depending on patient size. The dual-energy technique allowed a reduction of CM dose by 20% at similar radiation dose as the standard 120 kV protocol.
Study II	In this patient study, the protocols from Study I were used to reduce CM doses by 40–50%, depending on patient size, with maintained CNR in patients with a BMI-range of 15–36 kg/m^2. The size-specific dose estimates increased by 70%.
Study III	The study suggests that using LAT+AP localizer yields more consistent noise and radiation dose than a single AP. The effect was small, except for a subgroup of females with laterally protruding breast tissue, which may have been overexposed by about 57% in the thorax region.
Study IV	The results indicate that sub-mSv CT is feasible for morphological characterization of skeletal changes in areas with increased tracer uptake on bone scintigraphy, although a larger study is needed.

7 FUTURE ASPECTS

Many of the classical quantitative techniques and the related assumptions, some of which have been relied on in this thesis, will need to be reevaluated as the level of iterative technique used in image reconstruction increases. All major CT vendors today have implemented so-called model-based iterative reconstructions (MBIR) on their newer models. This will have large implications for optimization methods, because of the nonlinearity of these algorithms. Some of the effects are that the standard relationship between dose and noise no longer apply; the noise texture and image resolution become dose and location dependent; and resolution becomes dependent on object contrast. This complicated behavior makes it very difficult to generalize from specific measurements to clinical applications, meaning that we will need to rely much more on detection- or rating based methods, which will need to be more task specific than previously. For example, evaluating the performance of model- or human observers in phantom studies that are suitable to represent a specific clinical task (by use of for instance ROC analysis), or evaluating the fulfillment level of specific standardized image quality criteria in patient images (by using for instance visual grading characteristics (VGC) analysis). The properties of these MBIR algorithms may also have implication for the ATCMs, as it may no longer be suitable to use noise standard deviation as a target for the tube-current adjustment. Here too, detection-based metrics have been proposed [53]. It should also be expected that the introduction of narrow artificial intelligence (AI) will have large implications for optimization methods. It is likely that various forms of AI techniques, will be used in reconstruction algorithms (causing similar complications as discussed above). But the most important impact will probably be its increased use in detection and image recognition. In narrow image assessment tasks, it is already possible for deep-learning-based algorithms to reach superhuman capabilities. A striking recent example is an algorithm which, via an image of the retina, is able to predict the subjects age with a mean absolute error of 3.3 years, gender (AUC = 0.97), smoking status (AUC = 0.71), systolic blood pressure (mean absolute error 11.2 mmHG) and major adverse cardiac events (AUC = 0.70) [54]. Given the large potential of these techniques, it is therefore likely that much of image optimization will be aimed at producing image characteristics that are suitable for the detection- or image recognition algorithm, meaning that it will need to be incorporated in the work.

8 ACKNOWLEDGEMENTS

I would like to thank my main supervisor **Torkel Brismar** and my co-supervisors **Gavin Poludniowski** and **Marcus Söderberg** for all your contributions. Torkel for your support, enthusiasm and optimism, valuable knowledge and unprecedented ability to make things happen in the face of a deadline. Gavin for your support, helpfulness, valuable knowledge, scientific curiosity and the much-appreciated discussions. Marcus for your support, valuable knowledge, good ideas and the lowest average e-mail response-time ever observed. I would also like to thank my former boss and former co-supervisor **Agnetha Gustafsson** for allowing me to combine the Ph.D. education with work, and for the appreciated help I received while you were at Karolinska.

9 REFERENCES

1. Hsieh, J., *Computed Tomography – Principles, Design, Artifacts and Recent Advances*. 2 ed. 2009: SPIE.
2. Kalender, W.A., *Computed Tomography: Fundamentals, System Technology, Image Quality, Applications*. 2011: Publicis MCD Werbeagentur GmbH.
3. Kalender, W.A., et al., *Technical approaches to the optimisation of CT.* Phys Med, 2008. **24**(2): p. 71-9.
4. Poludniowski, G., et al., *SpekCalc: a program to calculate photon spectra from tungsten anode x-ray tubes.* Phys Med Biol, 2009. **54**(19): p. N433-8.
5. Lusic, H. and M.W. Grinstaff, *X-ray-computed tomography contrast agents.(Report).* Chemical Reviews, 2013. **113**(3): p. 1641-1666.
6. Attix, F.H., *Introduction to Radiological Physics and Radiation Dosimetry*. 2004.
7. Hua, C.-h., et al., *Accuracy of electron density, effective atomic number, and iodine concentration determination with a dual-layer dual-energy computed tomography system.* Medical Physics, 2018. **45**(6): p. 2486-2497.
8. Krauss, B., *Dual Energy Physics Lecture Notes*. 2012, Siemens: Erlangen.
9. Kulkarni, N.M., et al., *Determination of renal stone composition in phantom and patients using single-source dual-energy computed tomography.* Journal of computer assisted tomography, 2013. **37**(1): p. 37.
10. NIST. *X-Ray Mass Attenuation Coefficients*. 2019 2019-09-15; Available from: https://www.nist.gov/pml/x-ray-mass-attenuation-coefficients.
11. Greenberger, P.A., R. Patterson, and C.M. Tapio, *Prophylaxis Against Repeated Radiocontrast Media Reactions in 857 Cases: Adverse Experience With Cimetidine and Safety of ß-Adrenergic Antagonists.* Archives of Internal Medicine, 1985. **145**(12): p. 2197-2200.
12. Svensk uroradiologisk förenings kontrastgrupp. *Nationella rekommendationer*. 2017 [cited 2018 3 Oct]; Available from: www.sfmr.se/Files.aspx?f_id=145491.
13. ACR Committee on Drugs and Contrast Media. *ACR Manual on Contrast Media*. 2018 [cited 2018 3 Oct]; Available from: https://www.acr.org/-/media/ACR/Files/Clinical-Resources/Contrast_Media.pdf.
14. Kooiman, J., et al., *Meta-analysis: serum creatinine changes following contrast enhanced CT imaging.* Eur J Radiol, 2012. **81**(10): p. 2554-61.
15. Moos, S.I., et al., *Contrast induced nephropathy in patients undergoing intravenous (IV) contrast enhanced computed tomography (CECT) and the relationship with risk factors: A meta-analysis.* European Journal of Radiology, 2013. **82**(9): p. e387-e399.
16. McDonald, R.J., et al., *Intravenous Contrast Material-induced Nephropathy: Causal or Coincident Phenomenon?* Radiology, 2016. **278**(1): p. 306.

17. McDonald, R.J., et al., *Intravenous contrast material exposure is not an independent risk factor for dialysis or mortality.* Radiology, 2014. **273**(3): p. 714.

18. IEC. *Medical electrical equipment – Part 2-44: Particular requirements for the basic safety and essential performance of X-ray equipment for computed tomography (IEC 60601-2-44).* 2012; 3.1:[

19. ICRP, *The 2007 Recommendations of the InternationalCommission on Radiological Protection.* Annals of the ICRP, 2007.

20. Huda, W., D. Magill, and W. He, *CT effective dose per dose length product using ICRP 103 weighting factors.* Medical Physics, 2011. **38**(3): p. 1261-1265.

21. Stamm, G.D. and H.D. Nagel, *CT-Expo - ein neuartiges Programm zur Dosisevaluierung in der CT.* Röfo. Fortschritte Auf Dem Gebiet Der Röntgenstrahlen Und Der Bildgebenden Verfahren, 2002. **174**(12): p. 1570-1576.

22. ImPACT. *CT Dosimetry*. 2019 [cited 2019 14 Oct]; Available from: http://www.impactscan.org/ctdosimetry.htm.

23. AAPM Task Group 293, *Size-Specific Dose Estimate (SSDE) for Head CT.* American Association of Physicists in Medicine, 2019.

24. AAPM Task Group 204, *Size-Specific Dose Estimates (SSDE) in Pediatric and Adult Body CT Examinations.* American Association of Physicists in Medicine, 2011.

25. AAPM Task Group 220, *Use of Water Equivalent Diameter for Calculating Patient Size and Size-Specific Dose Estimates (SSDE) in CT.* American Association of Physicists in Medicine, 2014.

26. Wang, J., et al., *Attenuation-based estimation of patient size for the purpose of size specific dose estimation in CT. Part II. Implementation on abdomen and thorax phantoms using cross sectional CT images and scanned projection radiograph images.* Med Phys, 2012. **39**(11): p. 6772-8.

27. Wang, J., et al., *Attenuation-based estimation of patient size for the purpose of size specific dose estimation in CT. Part I. Development and validation of methods using the CT image.* Med Phys, 2012. **39**(11): p. 6764-71.

28. United Nations Scientific Committee on the Effects of Atomic Radiation, *UNSCEAR 2017 Report: "Sources, effects and risks of ionizing radiation".* United Nations Publication, 2018.

29. Brenner, D.J., *Cancer risks attributable to low doses of ionizing radiation: Assessing what we really know.* PNAS, 2003. **100**: p. 13761-13766.

30. United Nations Scientific Committee on the Effects of Atomic Radiation, *UNSCEAR 2010 Report: "Summary of low-dose radiation effects on health".* United Nations Publication, 2011.

31. Alliance for Quality Computed Tomagraphy Working Group. *Reference CT protocols*. 2015 [cited 2018 09 Oct]; Available from: https://www.aapm.org/pubs/CTProtocols/.

32. Strålsäkerhetsmyndigheten, *Strålsäkerhetsmyndighetens föreskrifter om medicinska exponeringar*, in *SSMFS 2018:5*, Strålsäkerhetsmyndigheten, Editor. 2018.

33. Committe to Assess Health Risks from Exposure to Levels of Ionizing Radiation, N.R.C., *Health Risks from Exposure to Low Levels of Ionizing Radiation: BEIR VII – Phase 2*. The National Academies Press, 2006.

34. Samei, E., M.J. Flynn, and W.R. Eyler, *Detection of subtle lung nodules: relative influence of quantum and anatomic noise on chest radiographs.* Radiology, 1999. **213**: p. 727-734.

35. Sund, P., L.G. Mansson, and M. Bath, *Development and evaluation of a method of calibrating medical displays based on fixed adaptation.* Med Phys, 2015. **42**(4): p. 2018-28.

36. Cherry, S.R., J.A. Sorenson, and M.E. Phelps, *Physics in Nuclear Medicine*. 4 ed. 2012: Elsevier.

37. Solomon, J. and E. Samei, *Correlation between human detection accuracy and observer model-based image quality metrics in computed tomography.* Journal of medical imaging (Bellingham, Wash.), 2016. **3**(3): p. 035506.

38. Aurumskjöld, M.-L., *Optimisation of image quality and radiation dose in computed tomography using iterative reconstruction*. 2017: Lund University, Faculty of Medicine Doctorial Dissertation Series.

39. McNitt-Gray, M. *Tube Current Modulation Approaches: Overview, Practical Issues and Potential Pitfalls*. 2011 [cited 2018 8 Oct]; Available from: https://www.aapm.org/meetings/2011CTS/documents/McNitt-GrayTubeCurrentModulationv4.pdf.

40. Merzan, D., et al., *Evaluating the impact of scan settings on automatic tube current modulation in CT using a novel phantom.* Br J Radiol, 2017. **90**(1069): p. 20160308.

41. Papadakis, A.E., K. Perisinakis, and J. Damilakis, *Automatic exposure control in pediatric and adult multidetector CT examinations: a phantom study on dose reduction and image quality.* Med Phys, 2008. **35**(10): p. 4567-76.

42. Soderberg, M., *OVERVIEW, PRACTICALTIPS AND POTENTIAL PITFALLS OF USING AUTOMATIC EXPOSURE CONTROL IN CT: SIEMENS CARE DOSE 4D.* Radiation Protection Dosimetry, 2016. **169**(1-4): p. 84-91.

43. Kaza, R.K., et al., *Emerging techniques for dose optimization in abdominal CT.* Radiographics : a review publication of the Radiological Society of North America, Inc, 2014. **34**(1): p. 4.

44. Yu, L., et al., *Optimal tube potential for radiation dose reduction in pediatric CT: principles, clinical implementations, and pitfalls.* Radiographics : a review publication of the Radiological Society of North America, Inc, 2011. **31**(3): p. 835.

45. Kalender, W.A., et al., *Application- and patient size-dependent optimization of x-ray spectra for CT.* Med Phys, 2009. **36**(3): p. 993-1007.

46. Menke, J., *Comparison of different body size parameters for individual dose adaptation in body CT of adults.* Radiology, 2005. **236**(2): p. 565.

47. Lell, M.M., et al., *Optimizing Contrast Media Injection Protocols in State-of-the Art Computed Tomographic Angiography.* Investigative Radiology, 2015. **50**(3): p. 161-167.

48. Bae, K.T., *Intravenous contrast medium administration and scan timing at CT: considerations and approaches.* Radiology, 2010. **256**(1): p. 32.

49. Burton, C.S. and T.P. Szczykutowicz, *Evaluation of AAPM Reports 204 and 220: Estimation of effective diameter, water-equivalent diameter, and ellipticity ratios for chest, abdomen, pelvis, and head CT scans.* J Appl Clin Med Phys, 2018. **19**(1): p. 228-238.

50. Lee, S.H., et al., *Diagnostic accuracy of low-dose versus ultra-low-dose CT for lumbar disc disease and facet joint osteoarthritis in patients with low back pain with MRI correlation.* Skeletal Radiol, 2018. **47**(4): p. 491-504.

51. Alshamari, M., et al., *Low dose CT of the lumbar spine compared with radiography: a study on image quality with implications for clinical practice.* Acta Radiol, 2016. **57**(5): p. 602-11.

52. Gleeson, T.G., et al., *Image quality in low-dose multidetector computed tomography: a pilot study to assess feasibility and dose optimization in whole-body bone imaging.* Can Assoc Radiol J, 2010. **61**(5): p. 258-64.

53. Khobragade, P., et al., *CT automated exposure control using a generalized detectability index.* Med Phys, 2019. **46**(1): p. 140-151.

54. Poplin, R., et al., *Prediction of cardiovascular risk factors from retinal fundus photographs via deep learning.* Nat Biomed Eng, 2018. **2**(3): p. 158-164.